Hydrological Processes

WILEY

RESEARCH ARTICLE OPEN ACCESS

Exploring the Relationship Between Groundwater Drought and Evapotranspiration With the JULES Land Surface Model in a UK Chalk Catchment

Sarah L. Collins[1] | Alberto Martínez-de la Torre[2,3] | Johanna Scheidegger[4] | Douglas B. Clark[2] | Andrew Hughes[4]

[1]British Geological Survey, Lyell Centre, Edinburgh, UK | [2]UK Centre for Ecology & Hydrology, Wallingford, UK | [3]Meteorological Surveillance and Forecasting Group, DT Galicia, Agencia Estatal de Meteorología (AEMET), A Coruña, Spain | [4]British Geological Survey, Environmental Science Centre, Keyworth, UK

Correspondence: Andrew Hughes (aghug@bgs.ac.uk)

Received: 6 February 2025 | **Revised:** 6 December 2025 | **Accepted:** 1 March 2026

Keywords: chalk | drought | groundwater | integrated modelling

ABSTRACT

Hydrological droughts can last months to years and impact large areas, leading to a multitude of ecological and socio-economic harm. The role of evapotranspiration (ET) in drought is very variable and there is contradicting evidence on the impact of anthropogenic warming on groundwater drought in the UK. We integrated a distributed groundwater model into the JULES land surface model (JULES-DGW) and simulated a chalk catchment in southern England over the period 1901–2015. The model showed a good match to river flows (Kling–Gupta efficiencies 0.73–0.83) and groundwater levels ($r^2 = 0.92$). We found a general trend of drying over time with small decreases in average moisture in the unsaturated zone and average groundwater levels, caused by increases in annual ET and decreases in recharge as a fraction of precipitation. The model suggests drier conditions in the unsaturated zone in late summer/early autumn in the late 20th–early 21st century have led to a delay in the recharge season. No increase in capillary rise was simulated throughout the modelling period and ET was found to decrease in most cases of severe drought, thus acting to limit the fall in groundwater levels.

1 | Introduction

Hydrological droughts can last months to years and impact large areas, leading to a multitude of ecological and socio-economic harms, including to water supply, crop production, river navigation and electricity production (Van Loon 2015). Climate change accelerates the terrestrial water cycle, as warming drives an increase in evapotranspiration (ET), causing more precipitation (J. Liu et al. 2013; Scheff and Frierson 2014). Increases in ET have caused an intensification of the dry season across large parts of the globe (Padrón et al. 2020), bringing more frequent and intense ecological and agricultural droughts since the 1950s, although there is little agreement regarding changes in northern Europe (IPCC 2023). In the near future, analyses indicate reducing low flows and increasing duration and severity of hydrological drought for much of the globe (e.g., Hari et al. 2020; C. Zhao et al. 2020; Spinoni et al. 2021; Gu et al. 2023).

Groundwater is the Earth's largest liquid store of freshwater. It plays a fundamental role in public water supply, irrigation and terrestrial ecosystems (Gleeson et al. 2012), sustaining baseflow to rivers, lakes and wetlands in periods of low rainfall. Groundwater comprises ~25% of all freshwater withdrawals (UN 2022) with an estimated 2.5 billion people solely dependent on its use (UNESCO 2015). Within the world's cities, groundwater use is intensifying, with just under 50% of the global urban population dependent on groundwater (Foster et al. 2020). Groundwater systems are inherently more resilient to climate variability, storing water from periods of surplus and, largely, protected from the evaporative losses suffered by reservoirs.

Globally, both rising and falling trends in groundwater levels are observed (Bonsor et al. 2018; Scanlon et al. 2022, 2023). Although human intervention is the primary driver, the impact of climate variability can also be observed (Taylor et al. 2013; Scanlon et al. 2023). Given our dependence on groundwater, groundwater droughts—that is, periods of abnormally low groundwater levels (Van Loon 2015)—are a major threat to global water security and are potentially being intensified by climate change (Bloomfield et al. 2019).

The contribution of ET to drought remains an active topic of debate (Dai 2011; Sheffield et al. 2012; Teuling et al. 2013; Milly and Dunne 2016; Lehner et al. 2017; He et al. 2022; M. Zhao et al. 2022; Gu et al. 2023; Z. Zhao et al. 2023), in a large part, because of a lack of high-quality long-term observations (Dolman and de Jeu 2010; Mueller et al. 2011; Chu et al. 2017). The ET anomaly can be either positive or negative during drought. A negative ET anomaly occurs when low soil moisture inhibits bare-soil evaporation and causes stomatal closure, limiting transpiration and the depletion of water storage (Jung et al. 2010; Seneviratne et al. 2010; Novick et al. 2016; Y. Liu et al. 2020; Gupta et al. 2020). Conversely, a positive ET anomaly has been found to occur where the warm and dry atmospheric conditions usually present during drought lead to an increase in ET, accelerating the depletion in water storage (Seneviratne et al. 2012; Teuling et al. 2013; Mukherjee et al. 2022; Z. Zhao et al. 2023). Factors that may affect the response of ET to drought include duration and intensity of drought, climate conditions and plant species (He et al. 2022). In studies that use drought indicators—such as the Palmer drought severity index or the standardised precipitation evapotranspiration index (SPEI)—the influence of ET can be highly dependent on the choice of indicator or method used to calculate potential ET (PET) (Wang et al. 2022), as well as on the quality of the meteorological data (Trenberth et al. 2014). The IPPC (2023) summarise the research in this area by attributing medium confidence to the statement that '... climate change has contributed to increases in agricultural and ecological droughts in some regions due to increased land evapotranspiration' since the 1950s.

Hydrological droughts can occur in all climate zones. The UK periodically suffers from severe droughts, which, although less extreme than in more arid regions of the world, nevertheless lead to major water shortages (Marsh et al. 2007; Barker et al. 2019), particularly where resources are managed with an expectation of plentiful supply. In Wales and Scotland, while groundwater is used little in public water supply, it is the only viable water source for many rural communities as well as being relied upon in agriculture and industry (Glendell et al. 2024; NRW 2024). In contrast, groundwater comprises approximately a third of public water supply in England, which increases to > 75% in the south-east, the centre of the UK population and economy (BGS 2024). The majority of this supply is from the Chalk, a microporous limestone that is a dual-porosity/dual-permeability medium and transmits water in the saturated zone mainly via fractures.

Projections of drought in the UK through the 21st century are reflective of global projections, with low flows expected to decrease leading to increases in drought duration, intensity and severity (e.g., Rudd et al. 2017; Kay et al. 2021; Chan et al. 2022; Parry et al. 2024). However, the picture for groundwater is more complex, in part because the propagation of meteorological to groundwater drought is influenced by land cover, soil type, the thickness of the unsaturated zone and lateral groundwater flow (Bloomfield et al. 2015; Chen et al. 2024). Jackson et al. (2015) projected lower summer groundwater levels and higher winter groundwater levels in the UK by the 2050s under the UKCP09 high emissions scenario. This analysis was extended and updated with UKCP18 projections by Parry et al. (2024), who found substantial variability in projections of low groundwater levels and groundwater drought characteristics across the UK. They suggested that groundwater is little impacted by warmer, drier summers, as recharge predominately occurs in the winter, which is projected to become wetter (Kendon et al. 2022; Parry et al. 2024). Their study, however, contradicts the observational study of Bloomfield et al. (2019), who found increases in the frequency, duration and severity of groundwater drought in two boreholes in the UK over the period 1891–2015. Bloomfield et al. (2019) attribute these increases to enhanced ET directly from groundwater stores where the water table is shallow or the capillary fringe is thick, a process not represented in the model used by Parry et al. (2024).

Given the importance of the Chalk for water supply and its potential vulnerability to meteorological droughts, it is necessary to understand what drivers are responsible for drought conditions. Understanding recharge to groundwater systems is key to understanding groundwater drought. A number of studies have been undertaken to investigate recharge processes and, in particular, how the unsaturated zone in the Chalk can attenuate the recharge signal. The dual-porosity nature of the Chalk (e.g., Price et al. 1993) means that it is challenging to represent recharge processes, as the matrix has a high porosity but very low permeability. This feature of the Chalk unsaturated zone means that drainage from storage to the water table can occur through the matrix even during dry periods with no excess precipitation (Butler et al. 2012). Modelling shows this process is sensitive to the hydraulic conductivity of the matrix and the near surface properties of the Chalk (Mathias et al. 2005), which are generally high porosity and permeability (a 'regolith' upper layer), providing enhanced storage and attenuation (Ireson et al. 2006, 2009). The ability of the matrix to hold water and release it slowly is thus key to understanding the resilience of groundwater to drought.

There is a long history of groundwater modelling of the River Kennet catchment given its importance for water supply and its 'research pedigree', particularly as part of the UK Natural Environment Research Council's Lowland Catchment Research project (known as LOCAR; Wheater et al. 2007) undertaken in the Pang and Lambourn (see Figure 2). The first model, developed in the 1980s, used a bespoke code to show the importance of including a vertical variation of hydraulic conductivity to simulate the hydrograph response (Rushton et al. 1989). Following on from this work, the British Geological Survey (BGS) developed a ZOOMQ3D model of the Marlborough and Berkshire Downs and south-west Chilterns, which covered the Kennet catchment (Jackson 2012). The model has since been used to investigate the impacts of differing regional climate models on climate change in the Chalk (Jackson et al. 2011), to investigate groundwater flooding (Collins, Christelis, et al. 2020) and in conjunction with a detailed well model to study the performance of abstraction

boreholes in Chalk catchments (Upton et al. 2020). Whereas these studies used a simple soil moisture balance model to generate recharge for a groundwater model, other studies in the Kennet have simulated the land surface and shallow subsurface with greater complexity with the Joint UK Land Environment Simulator (JULES). Le Vine et al. (2016) and Rahman and Rosolem (2017) both represented the dual-permeability nature of the Chalk: the former with a Brooks and Corey (1964) dual curve approach and the latter with a bulk conductivity model. Whereas Rahman and Rosolem (2017) did not use a groundwater model—with recharge instantaneously becoming subsurface runoff at the base of the soil column—Le Vine et al. (2016) applied a variable flow boundary to the bottom of the soil column to generate recharge for BGS's ZOOMQ3D model. None of the approaches described above truly integrates the soil zone with the saturated groundwater flow via the unsaturated zone. The corollary of this means that understanding all the components of the subsurface system and their interactions is not possible. To be able to address such questions as how drought propagates from the soil through to the saturated zone as well as the interaction with the atmosphere, a model that integrates all parts of the system is required. This is only possible with a model that links a land surface model, which includes soil–atmosphere interaction, the unsaturated and saturated zone, with the lateral movement of groundwater.

The aim of this study was to implement a groundwater model into the JULES land surface model that incorporates all processes that influence groundwater drought: lateral groundwater flow; river–aquifer interaction; groundwater abstraction; and capillary rise and recharge between the aquifer and unsaturated zone. The model was then used to simulate the Kennet—a catchment typical of those relied upon for water supply in the UK—and the contribution of ET to groundwater drought was explored.

2 | Data and Methods

2.1 | Implementation of a Groundwater Flow Model in the JULES

JULES is a widely used community land surface model that simulates fluxes of water, carbon, energy and momentum between the atmosphere and the land surface (Best et al. 2011; Clark et al. 2011). It is coupled to the UK's atmospheric model—the Met Office Unified Model—for operational weather forecasting and climate predictions. However, it can also be used as a standalone land surface model. Sub-grid heterogeneity in land use is handled with a tile-based approach, whereby the energy budget and canopy hydrology are calculated for each surface type within a cell (called a 'gridbox').

Soil moisture is treated as homogeneous across the gridbox. The soil column is typically split into four layers with thicknesses (from top to bottom) 0.1, 0.25, 0.65 and 2 m. A finite-difference approximation to the Richards equation is used to determine water fluxes between soil layers. The unsaturated hydraulic conductivity in each layer is estimated as a function of soil saturation by either the Brooks and Corey (1964) or the van Genuchten (1980) approach. The model produces surface runoff and subsurface runoff (essentially groundwater recharge). If no hydrology scheme is selected, surface runoff comprises only infiltration excess runoff, which is generated when the rainfall rate exceeds the infiltration capacity of the soil. Subsurface runoff is produced from the lowest soil layer at a rate equal to the hydraulic conductivity of that layer. Saturation excess surface runoff can be generated with the probability distributed model (PDM) (Moore 2007; Clark and Gedney 2008). The PDM approach in JULES calculates the saturated fraction (f_{sat}) of each gridbox as follows:

$$f_{sat} = 1 - \left[1 - \frac{\max\left(0, S - S_0\right)}{S_{max} - S_0}\right]^{\frac{b}{b-1}}$$

where b is a shape parameter, S is the gridbox soil water storage and S_0 is the minimum storage below which no saturation occurs. S_{max} is the maximum gridbox storage and calculated as follows:

$$S_{max} = \theta_{sat} \times dz_{pdm}$$

where θ_{sat} is the volumetric soil water content at saturation and dz_{pdm} is the depth of soil column over which the PDM model is applied (typically assumed 1 m). The saturation excess surface runoff is calculated by multiplying f_{sat} by the rate of precipitation/snow melt.

Given the nature of groundwater flows, that is, predominantly lateral, then there is a need to simulate how the subsurface runoff will be converted into horizontal flow between grid boxes. To do this, we implemented an explicit, two-dimensional, single-layer groundwater model in JULES. When the groundwater scheme is active, we turn off subsurface runoff and instead calculate a recharge flux or capillary rise between the lowest soil layer and the aquifer (see Figure 1). This vertical flux is then applied to the groundwater model, which calculates lateral flow between cells and baseflow to, or leakage from, rivers. The new JULES model with groundwater flow is referred to as JULES-DGW ('dynamic groundwater').

2.1.1 | Groundwater Model Formulation

The groundwater formulation is based on the LEAFHYDRO groundwater model (Fan et al. 2007; Miguez-Macho et al. 2007; Martínez-de la Torre and Miguez-Macho 2019), which calculates lateral flow on an octagonal grid with Darcy's law (see fig. 6 in Fan et al. 2007). The mass balance around a cell is formulated using the following equation:

$$\frac{dS_g}{dt} = \Delta x \Delta y R + \sum_{n=1}^{8} Q_n - Q_r$$

where S_g is the groundwater storage (kg); R is the flux between the groundwater and the soil zone ($kg\,m^{-2}\,s^{-1}$); $\Delta x \Delta y$ is the area of the grid box (m^2); Q_n is the lateral flow to/from the nth neighbour ($kg\,m^{-2}\,s^{-1}$) and Q_r is the groundwater-river exchange ($kg\,m^{-2}\,s^{-1}$). The flow between each cell can be described as follows:

$$Q_n = \frac{cT\left(\mathrm{wtd}_n - \mathrm{wtd}\right)}{l}$$

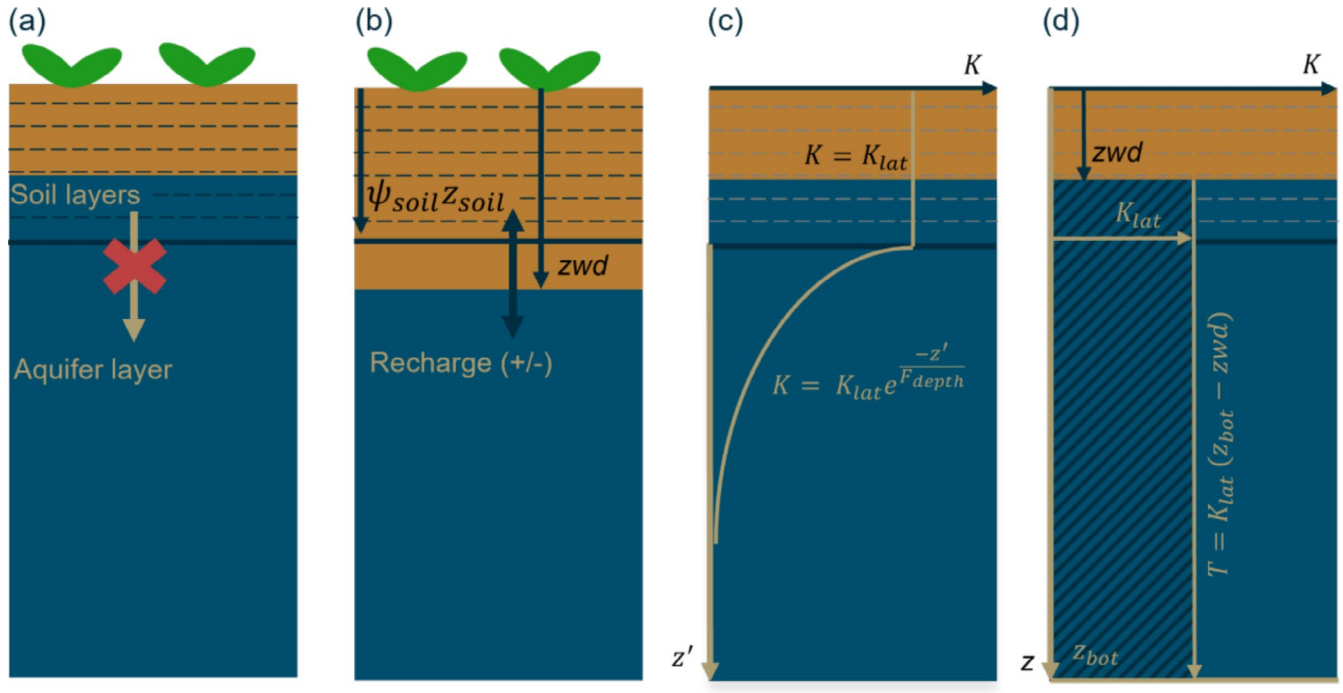

FIGURE 1 | JULES-DGW soil–groundwater interaction when (a) the water table is within the soil layers and (b) the water table is below the soil layers. Parameters in the calculation of transmissivity (T) for the two schemes: (c) with an exponential decrease in hydraulic conductivity (K) with depth and (d) a constant hydraulic conductivity with depth. F_{depth}, e-folding depth; φ_{soil}, matric potential of lowest soil layer.

where Q_n is the lateral flow between cells ($\text{kg m}^{-2}\text{s}^{-1}$); c is the cell width (m); transmissivity T ($\text{kg m}^{-1}\text{s}^{-1}$); wtd is the water table depth (n, neighbour) (m) and l is the distance between cells (m).

There are two different options for the calculation of T, which is defined as follows:

$$T = \int_{\text{zwd}}^{\infty} K_{\text{lat}} dz'$$

where K_{lat} ($\text{kg m}^{-2}\text{s}^{-1}$) is the hydraulic conductivity of the aquifer, zwd (m) is the depth to the water table and z' (m) is the depth of the water table below the top of the aquifer (see Figure 1c). The upper limit of the integral is infinity, as potentially, the ultimate depth of the water table is very large.

The first method of determining T assumes a constant hydraulic conductivity with depth until a defined base of the aquifer (z_{bot}) (Figure 1d):

$$T = \left(z_{\text{bot}} - \text{zwd}\right) \times K_{\text{lat}}$$

The second assumes an exponentially decreasing hydraulic conductivity with depth (Figure 1c), whereby T is calculated as follows:

If $F_{\text{depth}} \leq 1$:

$$T = 0$$

else if zwd > soil depth (m) (sd, Figure 1c):

$$T = F_{\text{depth}} \times K_{\text{lat}} \times e^{\frac{-(\text{zwd}-\text{sd})}{F_{\text{depth}}}}$$

else (i.e., water table within soil layers):

$$T = \left(F_{\text{depth}} - \text{zwd} + \text{sd}\right) \times K_{\text{lat}}$$

where F_{depth} (m) is the e-folding depth, z' (m) is the depth of the water table below the top of the aquifer and K_{lat} ($\text{kg m}^{-2}\text{s}^{-1}$) is, in this case, the maximum hydraulic conductivity at the top of the aquifer (Figure 1c). An exponential decrease in hydraulic conductivity with depth is widely used in hydrological modelling to simulate shallow groundwater, for example in TOPMODEL (Beven and Kirkby 1979). It tends to work best in catchments without a strong groundwater influence (Lane et al. 2019) because groundwater dominated catchments contain permeable rock or unconsolidated material and therefore permeability reduces more slowly with depth. While we envisage the constant conductivity with depth being more useful for most groundwater settings, an exponential decrease in conductivity with depth can be a good approximation to the conductivity profile in fractured aquifers: for example, hard-rock aquifers such as Gneiss (Collins, Loveless, et al. 2020) or in chalk (Rushton and Rathod 1981; Rushton et al. 1989).

2.1.2 | Soil–Groundwater Interaction

The interaction between the soil and groundwater is illustrated in Figure 1a,b. When the water table is below the base of the soil column, the equation of Niu et al. (2007) is used to calculate the recharge flux (q_r) as follows:

$$q_r = -K_{\text{soil}} \frac{-\text{zwd} - \left(\varphi_{\text{soil}} - z_{\text{soil}}\right)}{\text{zwd} - z_{\text{soil}}}$$

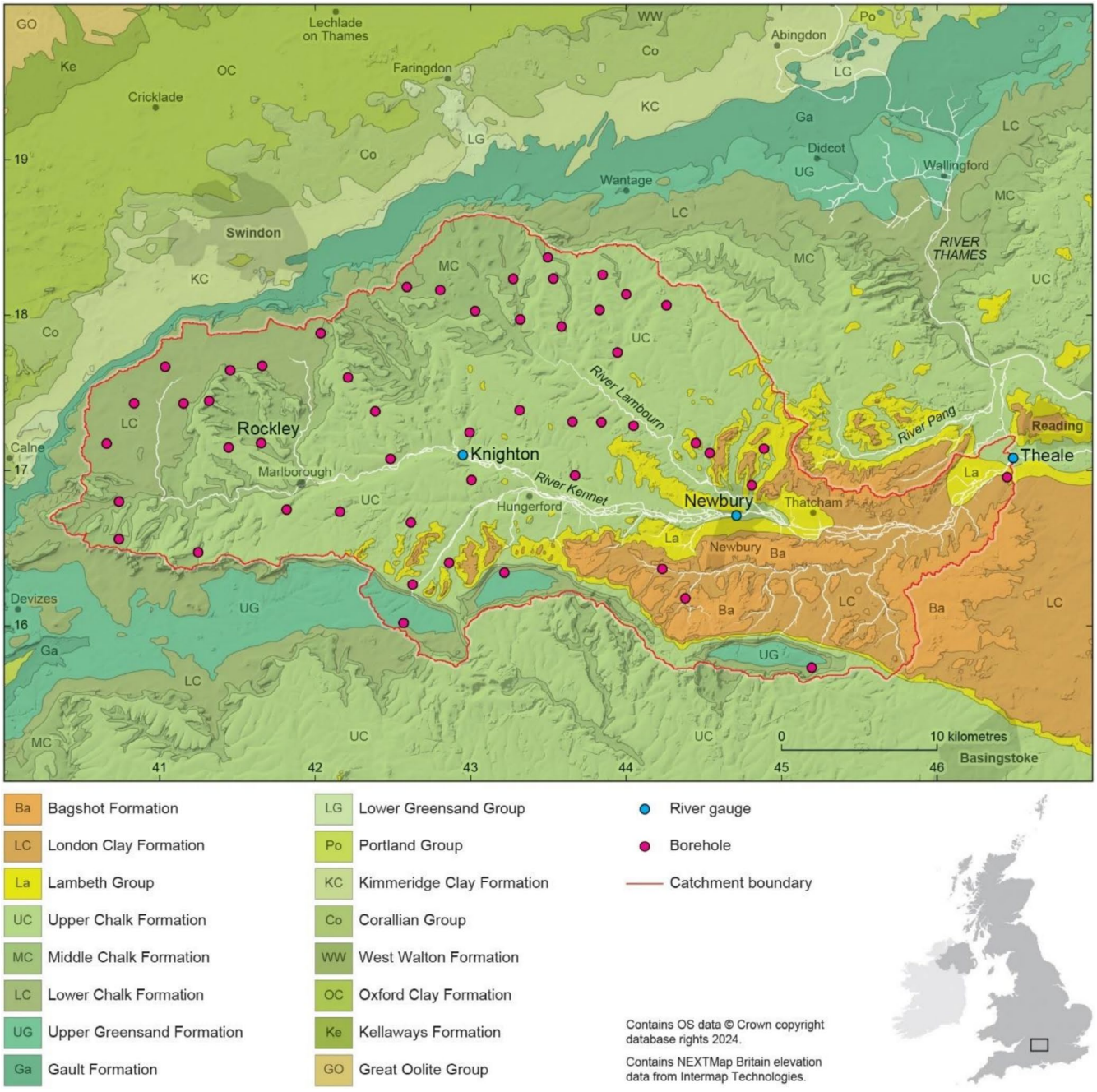

FIGURE 2 | The Kennet catchment geology, observation boreholes and river gauges.

where K_{soil} (kg m^{-2} s^{-1}) is the hydraulic conductivity of the lowest soil layer, z_{soil} (m) is the depth to the mid-point of the lowest soil layer and φ_{soil} (m) is the matric potential of the lowest soil layer. The amount of recharge that can occur in a single timestep is limited to the volume of water stored in the lowest soil layer. Batelis et al. (2020) found that averaging recharge between the recharge calculated for the current timestep and the recharge from the previous timestep increased stability and we employ the same approach here:

$$q_r^{t+1,i+1} = \frac{q_r^{t+1,i} + q_r^t}{2}$$

where t is the timestep and i is the number of iterations, which is set to one.

When the water table enters the soil column, we take the same approach as Batelis et al. (2020) and turn off the interaction between the aquifer and the soil column (Figure 1a). Instead, the position of the water table is estimated from the saturation of the soil layers. Any fluxes from river–groundwater interaction or abstraction are removed from the saturated soil layers, as well as the soil layer containing the water table, rather than from the aquifer.

2.1.3 | River–Groundwater Interaction

In JULES-DGW, flow between the aquifer and the river is proportional to the head difference and a river conductance term:

$$Q_r = C_{riv}\left(z_{riv} - \mathrm{zwd}\right)$$

where Q_r ($kg\,s^{-1}$) is groundwater baseflow or river leakage, z_{riv} (m) is the depth to the river below the surface and C_{riv} ($kg\,m^{-1}\,s^{-1}$) is the river conductance. When the groundwater level is below the base of the riverbed, this becomes:

$$Q_r = C_{riv}$$

assuming the river stage is 1 m above the base of the riverbed. A different river conductance can be chosen for influent and effluent conditions.

2.2 | Model Application

JULES-DGW comprises a relatively simple groundwater model, as it has been developed with large-scale modelling in mind. However, here we demonstrate its ability to model groundwater in a medium-sized catchment underlain by chalk, for which much validation data exist.

2.2.1 | Study Area

The Kennet catchment is located in southern England and encompasses an area of ~1030 km^2 (Figure 2). The river drains the Cretaceous Chalk of the Marlborough and Berkshire Downs, producing a slow response flow regime typical of groundwater catchments (baseflow index 0.88). To the south, the Chalk is overlain by Palaeogene deposits comprising the sands and gravels of the Lambeth group and the London Clay Formation. Whereas very little surface runoff occurs over the Chalk, significant runoff is generated where the low permeability London Clay Formation crops out (Figure 2). The Chalk is the most important aquifer in the UK, supplying ~70% of public water supply in south-east England (Jackson et al. 2011).

The Chalk is a dual-porosity, dual-permeability aquifer. The matrix has a high porosity, but this water is largely immobile due to the matrix's low permeability. Instead, fractures control the specific yield and transmissivity. Permeability is highest in the top of the aquifer and declines with depth as the frequency and aperture of fractures decline due to increasing overburden and a reduction in circulating groundwater and thus dissolution. The latter mechanism also results in larger fractures and therefore increased transmissivity close to rivers (Allen et al. 1997; MacDonald and Allen 2001). Recharge occurs slowly through the matrix; however, during heavy rainfall events, the fractures can become 'activated', leading to rapid rises in groundwater level (Ireson et al. 2009; Ireson and Butler 2011).

Land use within the catchment is predominantly rural, particularly over the Chalk downs, comprising a mix of arable land and grassland. Elevation ranges from ~45 m in the south-east to ~250 m in the west. Long-term average rainfall ranges from ~680 mm/year in the east to ~900 mm/year in the north (1961–2015).

2.2.2 | Kennet Model Setup

The Kennet catchment was extracted from a UK JULES configuration (Martínez-de la Torre et al. 2019) and the suite was developed into a JULES-DGW configuration (u-ba557). A summary of the model setup is provided in Table 1 and described in more detail below. The model extends beyond the Kennet east to the Thames (see Figure 2), as the groundwater divide between the Lambourn and Pang can move seasonally by up to 3 km (Jackson et al. 2006a). The boundaries conditions are no-flow around the edge of the model. The groundwater scheme was set up with the same 1 km^2 grid as the JULES model. Percentage land cover within each 1 km grid cell was extracted from the LCM2015 land cover map (Rowland et al. 2017). The van Genuchten (1980) approach was used to represent the hydraulic relationships between soil water content, suction and hydraulic conductivity. Soil hydraulic properties were adopted from the UK JULES model configuration (Martínez-de la Torre et al. 2019), which calculated soil hydraulic properties using pedotransfer functions (Wösten et al. 1999) and the Harmonised World Soil Database (FAO 2012), for the uppermost two layers. The remaining layers in the soil column were designated chalk and parameterised according to Le Vine et al. (2016), who derived the parameters from soil moisture–matric potential measurements in the Kennet. The disaggregation scheme (Williams and Clark 2014) was used to run JULES-DGW on a quarter-hourly time step, with convective precipitation occurring over a 2-h interval and large-scale precipitation over a 6-h interval.

The model was run for the period 1901–2015. Meteorological data for the period 1961–2015 were extracted from the CHESS-met dataset (Robinson et al. 2020). CHESS-met was developed specifically for providing driving data for JULES and provides all meteorological variables at a daily resolution on a 1 km^2 grid across the UK. For the period 1901–1960, precipitation data were extracted from HadUK 1 km gridded daily precipitation (Met Office et al. 2018). Surface air pressure varies only seasonally, and not interannually, in CHESS, and therefore the same seasonal values could be used for the 1901–1960 period. The remaining meteorological variables—temperature, wind speed, long/short wave radiation and specific humidity—were extracted from a single grid point in the WATCH dataset for 1901–1960 (Weedon et al. 2011). The 3-hourly WATCH data were aggregated to daily means as well as a daily temperature range. Temperature, radiation and specific humidity were applied uniformly over the catchment, whereas wind speed was varied spatially. Average spatial variation across the catchment in mean wind speed in CHESS (1961–2015) was applied to the period 1901–1960, while ensuring that the catchment mean was equal to the single-point values from WATCH. The period 1891–1901 was used as spin up. Precipitation was available for this period on a daily time step from HadUK (Met Office et al. 2018), but temperature was only available monthly (Met Office et al. 2018) and all other variables were estimated from seasonal means for the period 1901–2015.

The PDM was used to generate saturation excess runoff (Moore 2007). The model has two parameters, which are held constant across the domain: dz_{pdm}, the depth of soil considered by PDM; and b, a shape parameter. However, Bakopoulou (2015) grouped b across the Kennet according to HOST classification (Boorman et al. 1995) and then optimised b against river flows. In this study, we modified the JULES-DGW code to allow for spatial variation in b and parameterised b with the optimised

TABLE 1 | Details of model setup.

JULES input data type	Description	Source
Catchment grid	1 km^2 taken from GB JULES configuration; catchment outlines from the National River Flow Archive (NRFA)	See Martínez-de la Torre et al. (2019); NRFA—nrfa.ceh.ac.uk
Land use	Percentage land cover within each 1 km grid cell was extracted from the LCM2015 land cover map	See Rowland et al. (2017); https://doi.org/10.5285/6c6c9203-7333-4d96-88ab-78925e7a4e73
Soil properties	Soil hydraulic properties using pedotransfer functions and the Harmonised World Soil Database (FAO 2012), for the uppermost two layers. The remaining layers in the soil column were designated chalk; soil depth 0.35 m—UKSO	Upper layers: Pedotransfer functions: Wösten et al. (1999); HWSD (FAO 2012) Rest of model (chalk parametrisation) (Le Vine et al. 2016); UK Soil Observatory—https://mapapps2.bgs.ac.uk/ukso/home.html
Runoff generation	Probability distributed model or PDM; soil depth (dz_{pdm}) 1.0 m; shape parameter, b—distributed	Distributed values of b using optimised values of Bakopoulou (2015).
Saturated groundwater model	Transmissivity—exponentially decreasing values; specific yield 0.02; influent C_{riv} was extracted from Jackson et al. (2006b); initial conditions—groundwater head from Jackson et al. (2006b); Abstraction data from Thames Water	Fitted exponential curve to Transmissivity, river coefficient and initial heads based on Jackson et al. (2006b); Abstraction data—CEDA archive: https://doi.org/10.5285/18886f95ba84447f997efac96df456ad
Meteorological inputs	1961–2015: Daily, 1 km CHESS data	CHESS-met dataset (Robinson et al. 2020); https://eidc.ceh.ac.uk/login?came_from=/licences/archive/chess-met/
	1901–1960: HadUK 1 km gridded daily precipitation; temperature, wind speed, long/short wave radiation and specific humidity were extracted from a single grid point in the WATCH dataset	HadUK 1 km gridded daily precipitation (Met Office et al. 2018); www.metoffice.gov.uk/research/climate/maps-and-data/data/haduk-grid/datasets; WATCH dataset for 1901–1960 (Weedon et al. 2011)
Observations	Daily river flow data; soil moisture at Warren Farm (Environmental Information Data Centre—EIDC) Groundwater levels at observation boreholes	http://www.ceh.ac.uk/data/nrfa/data/search.html; EIDC—https://doi.org/10.5285/450bb14b-c711-47af-8792-f9bd88482cd4 National Groundwater Level Archive: http://www.bgs.ac.uk/research/groundwater/datainfo/levels/ngla.html; Environmental Agency data portal

values of Bakopoulou (2015). The parameter dz_{pdm} was set to 1.0 m.

A 3.85 m soil column was used: 1 0.1 m layer at the top and 15 0.25 m soil layers underneath. The two uppermost layers (0.35 m) are assumed to be soil above chalk. The soil depth was estimated from borehole records (UKSO, https://mapapps2.bgs.ac.uk/ukso/home.html), which show topsoil depths typically 10–40 cm. Rahman and Rosolem (2017) showed that the chalk unsaturated zone in the Kennet could be better represented by a bulk conductivity model (Zehe et al. 2001), which approximates the control fractures have on recharge by increasing saturated hydraulic conductivity (K_s) by many orders of magnitude above a certain threshold of soil saturation (S_0):

$$K_{sb} = K_s f_m \frac{S - S_0}{1 - S_0} \text{ if } S > S_0$$

$$K_{sb} = K_s \text{ if } S \leq S_0$$

where f_m [−] is a macroporosity factor and S [−] is the relative soil saturation. The bulk conductivity model was written into JULES-DGW. Rahman and Rosolem (2017) calibrated K_s, f_m and S_0 based on literature ranges. We used their values for K_s

and f_m, but found that their initial estimate of S_0 (0.8), which was based on the observed soil moisture–matric potential relationship in the Kennet, produced better river flows than their calibrated value (0.46).

An exponential decrease in hydraulic conductivity within the aquifer was used to reflect the distribution of fractures with depth (Figure 1c). Jackson et al. (2006b) calibrated hydraulic conductivity in the Kennet across three layers. In this study, we fitted exponential curves to every grid cell in Jackson et al.'s (2006b) model, such that transmissivity at the top of each layer would match as closely as possible between the two models. The fitting process was undertaken by taking each model node in the ZOOMQ3D model instance and determining the vertical T distribution, then ensuring that the exponential relationship was fitted using the 'curve_fit' function in SciPy toolbox. Specific yield was set to 0.02 across the catchment, which is a simplification given that specific yield in the Chalk varies both with depth and spatially in the range ~0.01–0.03 (Jackson et al. 2006b). With regard to the river–aquifer interaction, influent C_{riv} was extracted from Jackson et al. (2006b). The effluent C_{riv} was set to 0, inhibiting any inflow from the river into the aquifer. Abstraction data were obtained from the water company, Thames Water. These data showed total abstraction in the model (expressed as total volume per model area) increased from 0.04 mm/day between the start of the run (1894 to 1969) to around 0.07 mm/day in 1994 Initial groundwater levels were set from a steady-state simulation performed by Jackson et al. (2006b).

2.2.3 | Kennet Water Balance and Drought Analysis

We analysed the water balance and the evolution of drought through the 20th century and into the beginning of the 21st century. We re-ran the model without abstraction to obtain naturalised conditions. Following the methodology of Bloomfield et al. (2019), we split the outputs into three roughly equal periods (38, 38 and 39 years): 1901–1938, 1939–1976 and 1977–2015. Anomalies were calculated for precipitation, river flow and ET; for example, for precipitation:

$$P' = P - \overline{P}$$

where P is the monthly precipitation, $\overline{P}$ is the long-term (1901–2015) mean for that month and P' is the precipitation anomaly. The standardised groundwater index (SGI), precipitation index (SPI) and SPEI were all calculated with the standardised drought index toolbox in MATLAB (HRL 2024). The toolbox is based on a non-parametric framework (Farahmand and AghaKouchak 2015), and therefore provides a statistically consistent drought indicator across the different variables.

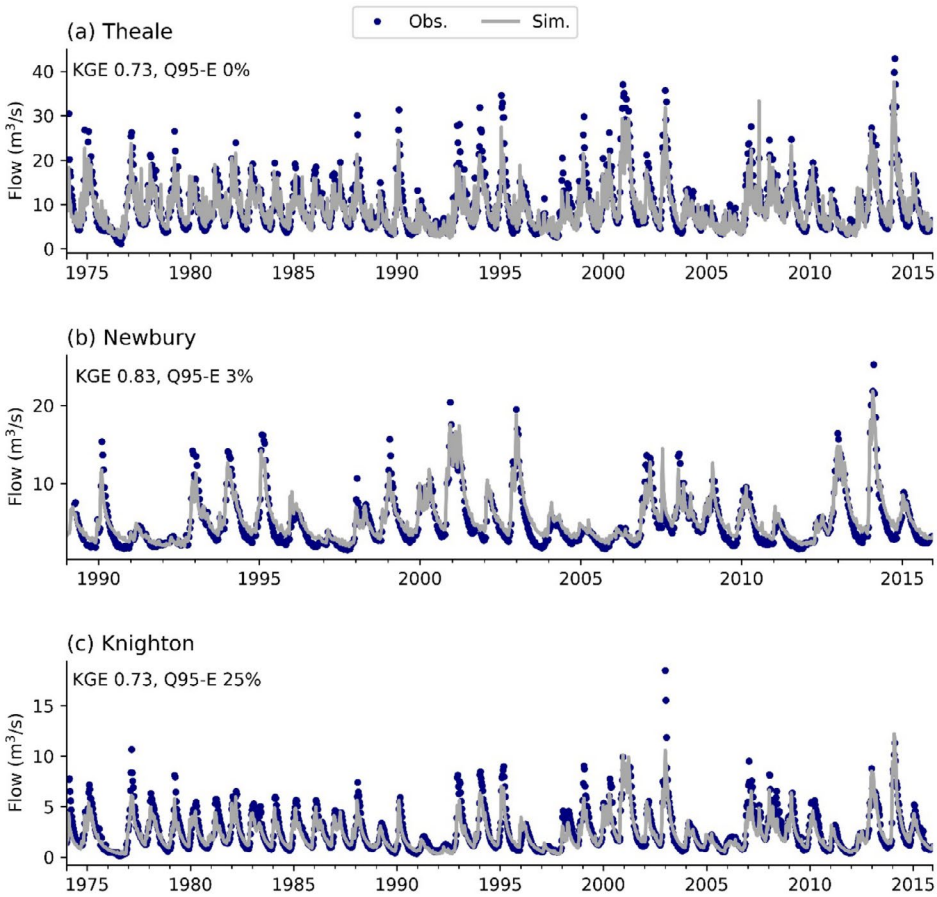

FIGURE 3 | 10-day mean observed and simulated river flow at (a) Theale, (b) Newbury and (c) Knighton. KGE, Kling-Gupta efficiency; Q95-E, percentage error in Q95. Contains data from *UK National River Flow Archive*.

3 | Results and Discussion

3.1 | Model Performance in the Kennet

A comparison of 10-day river flows between the model and observations at Theale, Newbury and Knighton is shown in Figure 3. We compare 10-day flows, rather than daily, because we have not included any routing in the model and the streamflow at the gauge is the summed groundwater baseflow and surface runoff over the catchment area (as in Le Vine et al. 2016). The model produces a good fit to streamflow with Kling-Gupta efficiencies between 0.73 and 0.83. However, it can be seen in Figure 3 that the model underestimates larger peaks at all three sites. The model is particularly good at simulating low flows, with an error in Q95 very close to 0% at Theale and 3% at Newbury.

Figure 4 shows the comparison between the soil moisture for the Sheepdrove Farm neutron probes, at the Warran Farm site in the north of the model area. The two soil moisture time series, located at 0.1 and 3.85 m below ground level, show how the soil

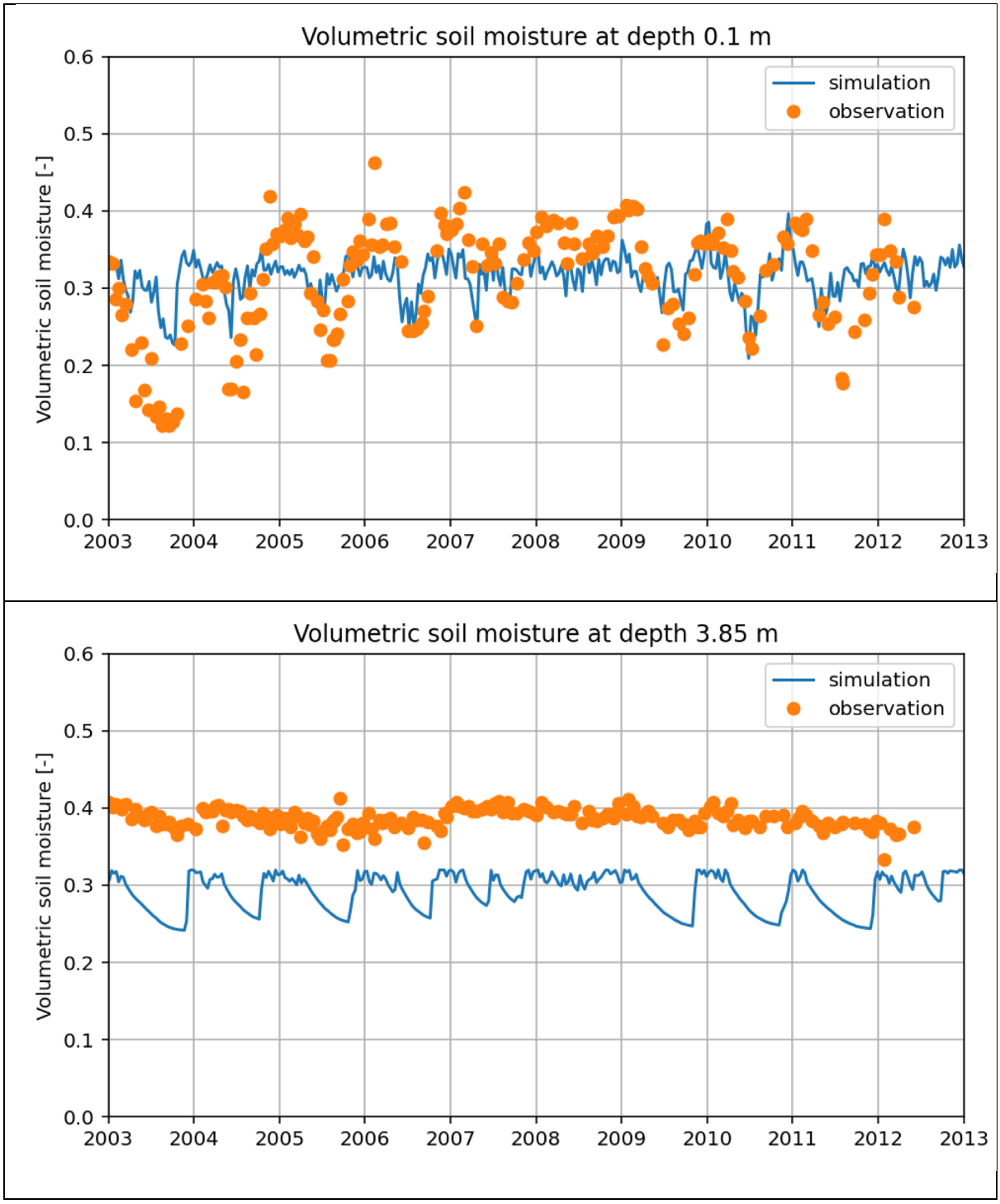

FIGURE 4 | Soil moisture response at Warren Farm soil moisture (Sheepdrove Farm) (a) depth of 0.1 m and (b) depth of 3.85 m (data available from EIDC; https://doi.org/10.5285/450bb14b-c711-47af-8792-f9bd88482cd4).

responds to seasonal differences in the balance between rainfall and evaporation by wetting and drying during the year, with higher soil moisture in the winter. While the range of the modelled soil moisture changes are underestimated in the shallower response and overestimated in the deeper one, the general seasonal response is reproduced.

Figure 5 shows the fit of the model to groundwater levels at 52 boreholes across the catchment (see Figure 2). Overall, the fit is good with a coefficient of determination $r^2 = 0.92$. However, at some boreholes the simulated groundwater levels deviate from the observations by 10–20 m. This is, in part, because we are comparing point observations with a model on a 1 km grid, but also because of the highly heterogeneous nature of the fractured aquifer. The observed groundwater levels show some large variations in boreholes a short distance apart or in the same grid cell. Figure 6 shows a comparison between observed and simulated SGI at Rockley, for which there is a particularly long observation record. We can see from Figure 6 that the model is able to simulate fluctuations in groundwater level over time. The fit appears to improve from the ~1970s. Of note is the winter of 1960/61, where the observed SGI suggests a very wet period (SGI > 2), whereas the model shows the opposite (SGI < −1). A discrepancy as large as this is likely an issue with the rainfall data and, similarly, the improvement in model fit in the second half of the 20th century is likely due to improved rainfall data, as more rain gauges were installed (Keller et al. 2015).

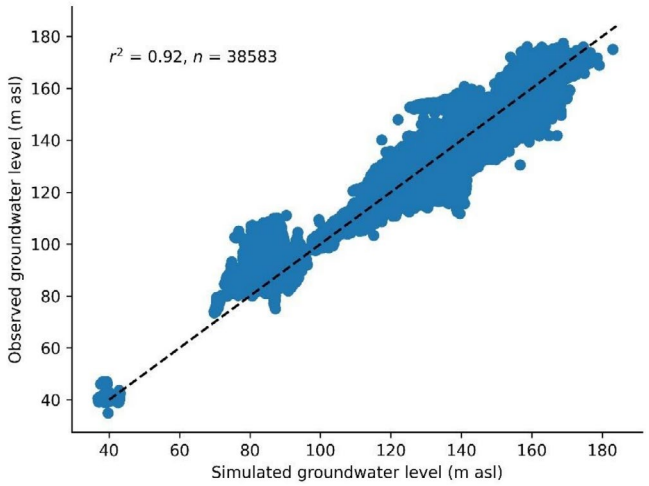

FIGURE 5 | Simulated versus observed groundwater levels within the Kennet. Dotted line shows line of perfect fit. asl, above sea level. Contains Environment Agency copyright and/or database right 2015.

One of the first groundwater models of the study area was presented by Rushton et al. (1989) and they produced a single-layer groundwater flow model and was driven by recharge estimate (Penman–Grindley). Their model simulates groundwater heads and baseflow to the river showing a reasonable fit, but head difference of up to ~10 m, particularly during the 1975/1976 drought event. Jackson (2012) extended this approach using the ZOOMQ3D model code—which is an advancement of Rushton's original but with adaptive time stepping to simulate shorter events better, that is, groundwater flooding. Both of these approaches used a vertical variation of hydraulic conductivity with depth which is adopted here. Use of JULES in the catchment has been specifically aimed at improving both soil processes

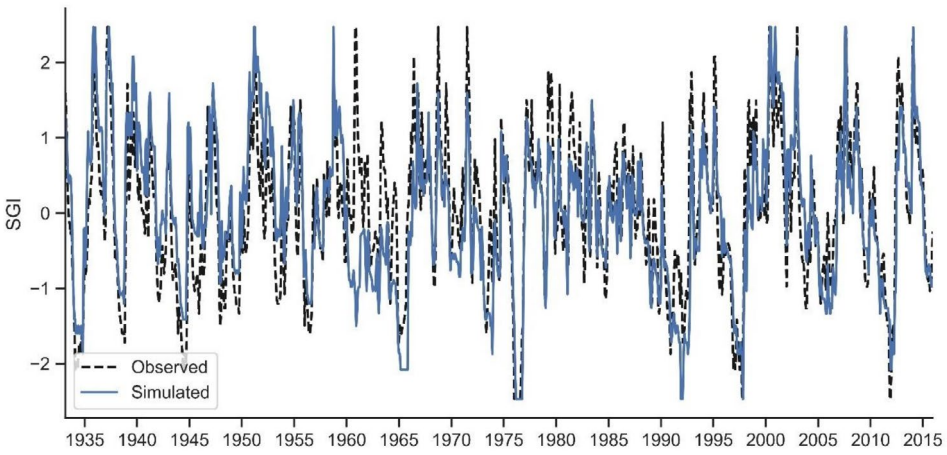

FIGURE 6 | Observed versus simulated standard groundwater level index (SGI) at borehole Rockley in the Kennet catchment.

TABLE 2 | Simulated mean (interquartile range) annual water balance (mm/a).

Water balance component	1901–1938	1939–1976	1977–2015
Precipitation	832 (759–901)	803 (716–901)	798 (705–862)
Evapotranspiration	486 (468–507)	474 (460–486)	490 (470–511)
Baseflow	285 (228–344)	269 (238–301)	251 (217–293)
Surface runoff	61 (52–65)	60 (51–66)	58 (50–66)

Note: Model water balance accurate to 0.1%.

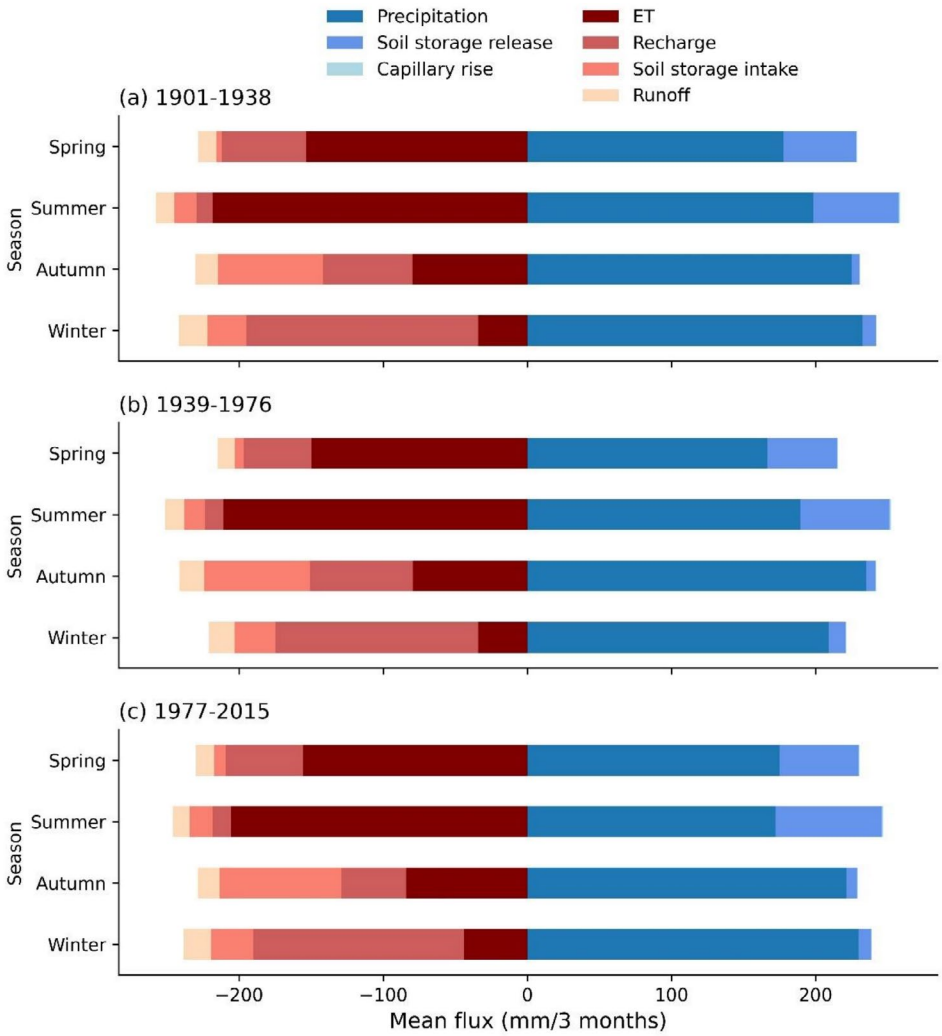

FIGURE 7 | Simulated mean seasonal water balance of unsaturated zone. Soil storage intake/release refers to the increase in soil moisture due to precipitation or capillary rise or decrease due to evapotranspiration (ET), surface runoff or recharge.

and groundwater: Le Vine et al. (2016) combined JULES with the ZOOMQ3D model instance presented by Jackson (2012) and showed that the water balance is similar to that presented here (see Section 3.2 below) as well as reproducing the groundwater hydrographs. All of these model instance show similar responses to that presented in this paper. The main departure is presented in Rahman and Rosolem (2017) who proposed a new formulation for JULES for the chalk but didn't include lateral groundwater flow. Their results showed good presentation of the soil/unsaturated zone, but they were not able to simulate groundwater heads and didn't include lateral flow. Therefore, the approach presented here, while based on a parsimonious groundwater flow model does reproduce the observed behaviour of the aquifer, but allows the unsaturated zone to be simulated and importantly provides both vertical integration of different subsurface components as well as allowing lateral groundwater flow.

3.2 | Kennet Water Balance

With climate change, winter precipitation in the UK is expected to increase in the order of 15% (Government Office for Science 2024). Long-term observations back to 1766 indicate no trend in UK annual precipitation, but a change in seasonality with wetter winters and drier summers (Alexander and Jones 2001). However, more recent meteorological data between 1961 and 2012 show significant trends only in Scotland, where annual and winter precipitation have both increased (Jenkins et al. 2008; Robinson et al. 2017). There has been an observable increase in evaporation, particularly in spring (Robinson et al. 2017). We re-ran the Kennet model without abstraction to look at the change in water balance over the period 1901–2015. Similarly to Bloomfield et al. (2019), to analyse the results over time, we split the outputs into three roughly equal periods (38, 38 and 39 years): 1901–1938, 1939–1976 and 1977–2015. The annual mean water balance is summarised in Table 2 and broken down by season for the unsaturated zone in Figure 7. Seasons in Figure 7 are the UK's meteorological seasons: spring—March, April, May; summer—June, July, August; autumn—September, October, November; winter—December, January, February. In the Kennet catchment, we see a decrease in mean annual precipitation across the three periods (832, 803 and 793 mm/a). Mean winter precipitation is similar in the first (232 mm) and third periods (229 mm) and lowest in the second period (209 mm). Mean

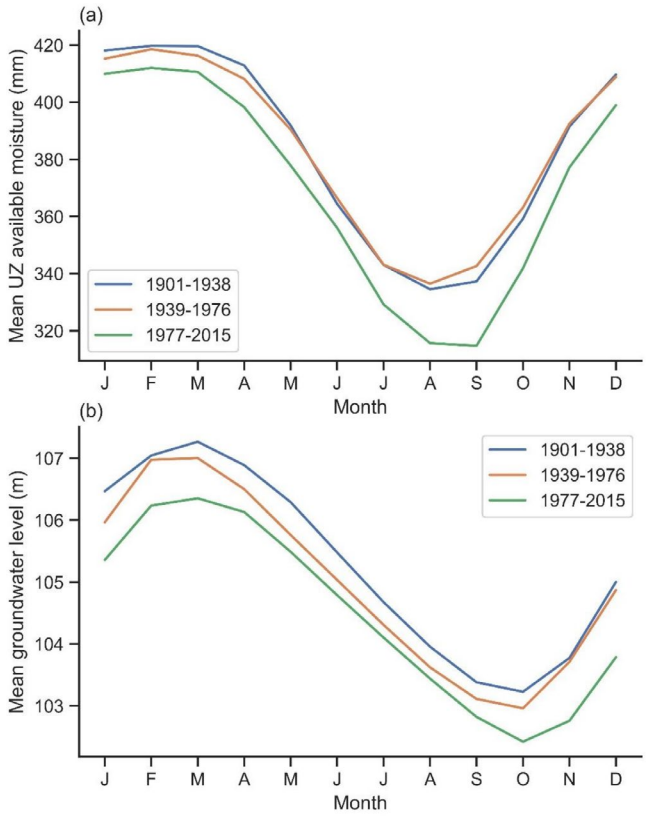

FIGURE 8 | Mean simulated groundwater levels and available moisture in the unsaturated zone (UZ) over the three periods.

summer precipitation decreased across the three periods (198, 189 and 172 mm).

Simulated mean annual ET was highest in the most recent period (490 mm/year) and lowest in the second period (474 mm/year) (Table 2) and has increased as a fraction of precipitation from 58% to 59% to 61%. Summer ET decreased across the three periods (218, 211 and 205 mm/year), but increased as a fraction of precipitation from 110% to 111% to 119%. The additional water required for ET is provided in the model by the release of storage from the soil/shallow unsaturated zone rather than from the saturated zone (Figure 7). Across the three periods, there is an increase in summer soil storage release from 59 to 62 to 74 mm. Capillary rise is very small and changes little among the three periods, reaching a maximum of 1 mm in summer. In autumn we see an increase in soil storage intake in the third period because the soil is drier at the beginning of the season due to lower summer precipitation: 73, 73 and 84 mm, which equates to 32%, 33% and 37% of autumn rainfall.

Simulated annual recharge decreases across the three periods (Figure 7), resulting in decreasing mean annual baseflow from 285 to 269 to 251 mm (Table 2). Annual baseflow as a fraction of rainfall also decreases: 34% to 32% to 30%. Autumn recharge is lowest in the third period: 62, 71 and 45 mm, which as fractions of rainfall are 28%, 30%, 20%. As mentioned above, the summers are, on average, drier in the third period, meaning the soil takes longer to wet up in the autumn and the recharge season is delayed. Winter recharge is highest in the first period and lowest in the second period: 161, 141 and 146 mm. As a fraction of rainfall, winter recharge decreases from 69% to 67% to 64%. Winter ET increases as a fraction of precipitation: 15% to 16% to 19%.

Figure 8 shows mean simulated available moisture in the unsaturated zone and groundwater levels for each of the three periods. Mean available moisture in the unsaturated zone is very similar between the first two periods. However, the model simulates less moisture in the unsaturated zone throughout the year in the third period. The difference is greatest at the end of summer/beginning of autumn in August/September, but despite high winter precipitation, moisture levels fail to reach saturation, in part due to high winter ET, which is 34 mm in the first two periods and 44 mm in the third. We also simulate a drop in groundwater levels throughout the year across the three periods (Figure 8b).

For the three periods (1901–1938, 1939–1976 and 1977–2015) examined as part of the historical simulation, an unsaturated zone balance (precipitation, soil moisture, capillary rise versus ET, recharge, soil moisture and runoff) and a groundwater balance: precipitation, ET, baseflow and runoff has been undertaken. Examining the changes over the three periods: the unsaturated zone shows limited capillary rise but no overall changes with time; the groundwater balance shows decreasing precipitation, variable ET (decreasing for the second period) and baseflow decreasing with surface runoff staying the same. Soil moisture and groundwater levels appear to decrease over the three periods, with the most pronounced change in the most recent period (1977–2015).

3.3 | Kennet Drought Periods

The SPI was calculated for all accumulation periods up to 24 months and found to be most strongly correlated with the SGI at an accumulation period of 16 months (SPI-16) ($r = 0.85$). Figure 9 shows the SPI-16 and SGI for the whole simulation period (1901–2015). The SPEI was also calculated for all accumulation periods up to 24 months and found to be most strongly correlated with the SGI at an accumulation period of 17 months (SPEI-17) ($r = 0.87$). Given that SPI-16 and SPEI-17 have very similar correlation with SGI (0.85 vs. 0.87, respectively), it appears that ET plays a very limited role in groundwater level fluctuations. Moreover, it can be seen in Figure 9 that, during periods of severe drought, SPEI is no better a predictor of SGI than SPI.

The observations show a decrease in average SPI-16 over the simulation period, which is reflected in a fall in average modelled SGI: SPI-16 0.3, −0.05, −0.17 and SGI 0.25, −0.03, −0.09 across the three periods (1901–1938, 1939–1976 and 1977–2015). Periods of severe drought—defined as a period of negative SPI-16 or SGI reaching −2—are highlighted in Figure 9. There are two such events in the first period, three in the second and four in the final period. All but two of these droughts were described as major hydrological droughts in the UK (Marsh et al. 2007; Barker et al. 2019), with the exceptions being those in 1944 and 1964–1966. The severe droughts in the final period are notably longer than in the first two periods: 18 and 28 months in the first, 13, 15 and 28 months in the second and 29, 33, 37 and 39 months in the final period.

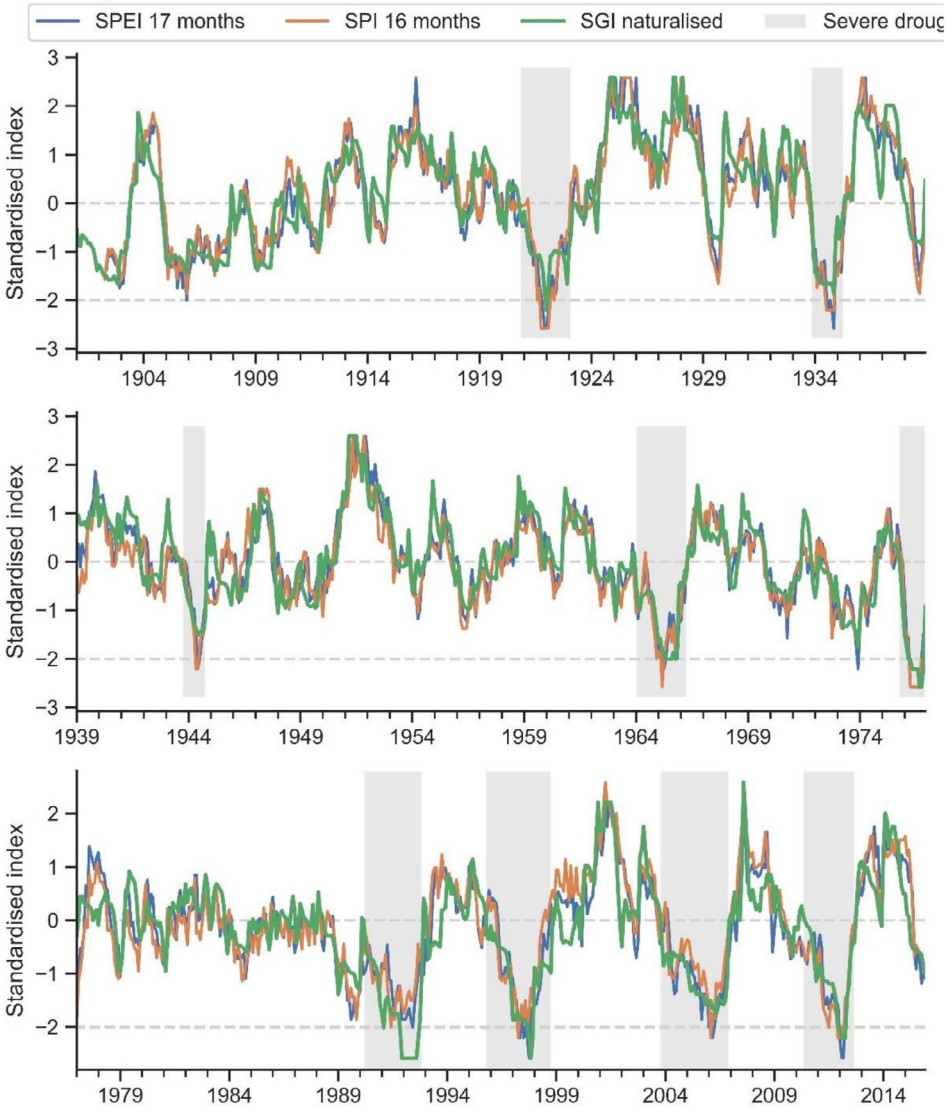

FIGURE 9 | Standardised indices for (simulated) groundwater level (SGI), (observed) precipitation with 16-month accumulation (SPI) and (observed) precipitation and (simulated) evapotranspiration with 17-month accumulation (SPEI). Severe droughts highlighted are those that reach −2 in SPI or SGI.

Figure 10 shows the evolution of these severe droughts in terms of anomalies from the point at which SGI drops below 0 to the point at which recovery begins. By comparing the plots with and without the ET anomaly (ET′) we can see that in seven of the nine events ET reduces the severity of the drought, that is, ET is lower than average (negative anomaly). This is perhaps because of the long duration of these groundwater droughts, and contrasts to observational evidence across Europe that shows a positive ET′ for single-year summer droughts (Teuling et al. 2013). According to the model, ET made a clear contribution to exacerbating the 2004–2006 drought and had neutral impact on the 1995–1998 drought, the two longest drought periods. The 2004–2006 drought is unusual in that the precipitation anomaly is largely positive during the first ~1 year, which maintained soil moisture and thus a positive ET′ developed. Groundwater storage in 2004 is low despite the positive precipitation anomaly because the preceding summer of 2003 was warm and dry and the unsaturated zone had a large deficit into the autumn, delaying the onset of the recharge season.

Figure 11 shows the degree of saturation in the soil (< 0.35 m bgl) and chalk (> 0.35 m bgl) for a gridbox with a shallow water table during the severe drought event of 1921/1922. From February 1921 there is a drop in the water table, but this is predominately due to lateral groundwater flow rather than capillary rise, and therefore a moisture deficit builds in the soil and upper chalk layers. When saturation in the chalk above the water table drops below 0.8—the threshold in the bulk conductivity model—the hydraulic conductivity becomes very small, which limits the upward movement of water from the water table to the soil zone. On the other hand, as the groundwater level is high, aquifer transmissivity is high and groundwater flows into neighbouring cells and towards nearby river cells. The lack of capillary rise is highlighted in Figure 12a, which shows that the available moisture in the

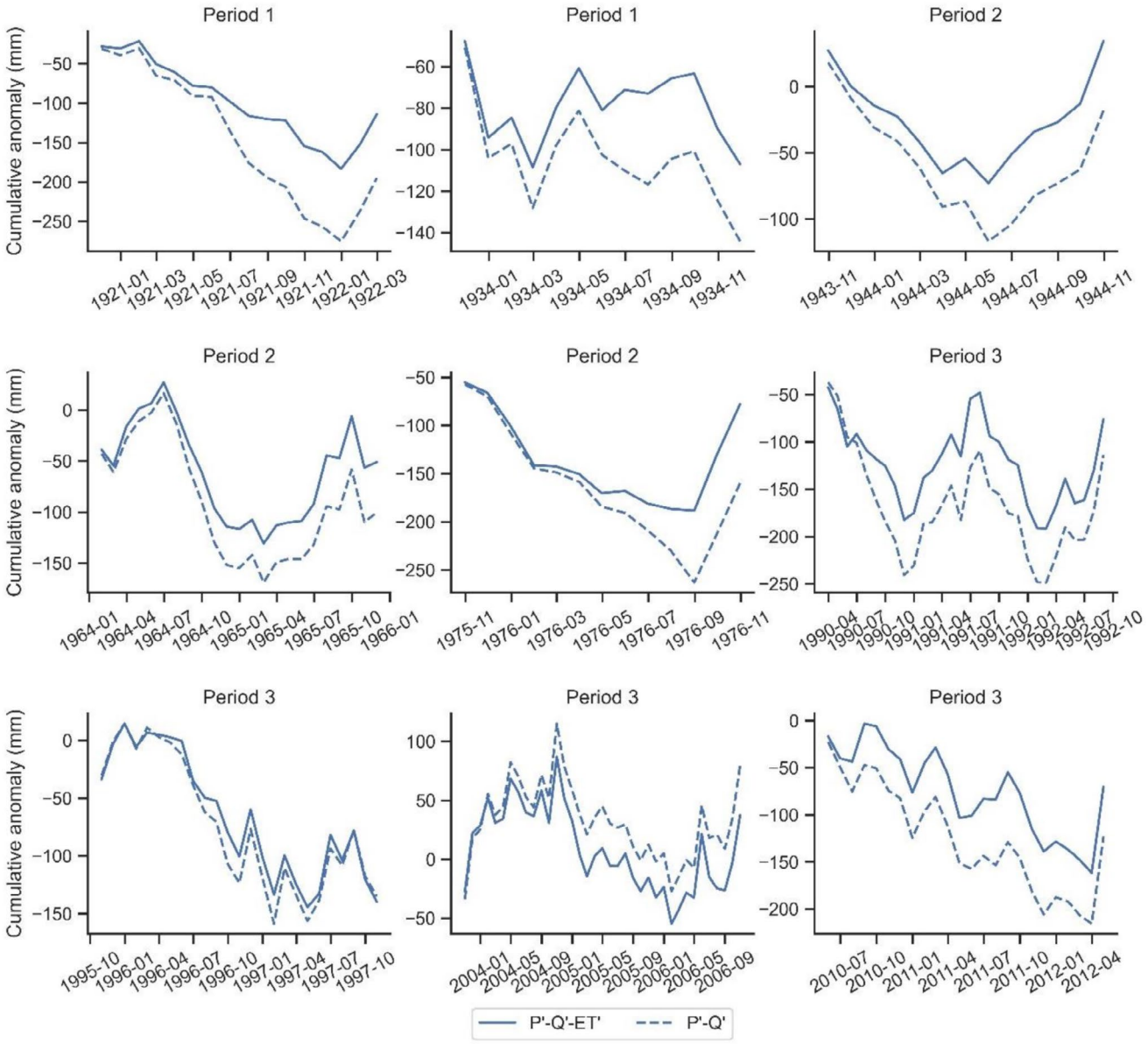

FIGURE 10 | Evolution of nine severe groundwater droughts illustrated by cumulative anomalies. *P′*, precipitation anomaly; *Q′*, discharge anomaly; ET′, evapotranspiration anomaly. Period 1: 1901–1938; period 2: 1939–1976; period 3: 1977–2015.

uppermost 1 m of this gridbox with a shallow groundwater level is no different from the catchment average during the summer months of highest ET, and the catchment average groundwater level is > 30 m. The moisture deficit in the unsaturated zone, therefore, restricts ET, which is well below potential ET as calculated with Penman–Monteith (Figure 12b). The similarity between localised and catchment behaviour demonstrates that the limiting factor on ET during droughts is the vertical movement of water.

This section has presented the evidence for the role of ET during historical droughts. By comparing time series of SPI-16, SPEI-17 and SGI, we demonstrate that these are strongly correlated and that SPI-16 is a predictor of SGI. Further, plotting the ET anomaly for individual drought events during the model simulation period demonstrates that evaporation typically reduces the severity of the drought rather than exacerbating it. The exception is the 2004–2006 drought event where ET anomaly increases the drought impact, although this drought is different in nature to previous events. Further exploration of the relationship between water stored in both the unsaturated and saturated zones and drought response would be beneficial; however, the current code allows the inclusion of lateral groundwater flow, which is a significant departure from previous integrated models applied in this catchment.

4 | Conclusions

We built a single-layer, distributed groundwater model into the JULES land surface model, named JULES-DGW. We made two further modifications to the code to simulate a chalk catchment: (1) spatially variable PDM parameters and (2) a bulk conductivity model in the unsaturated zone to represent the dual-permeability

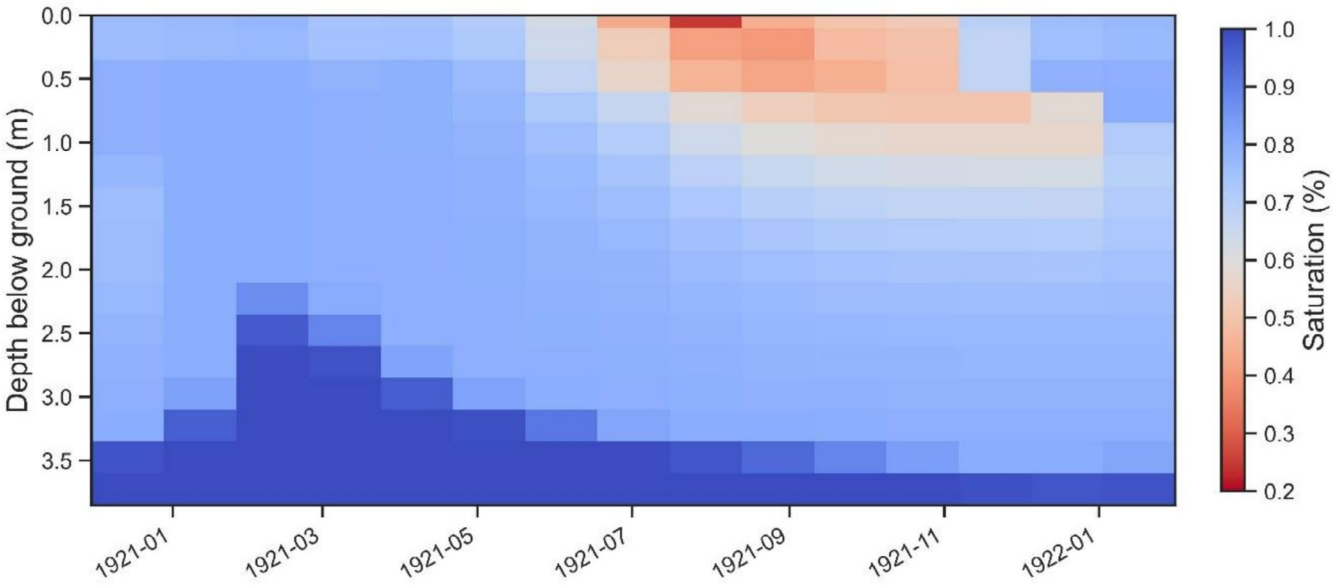

FIGURE 11 | Moisture in the unsaturated zone in a gridbox with a shallow water table for severe groundwater drought event in 1921/1922.

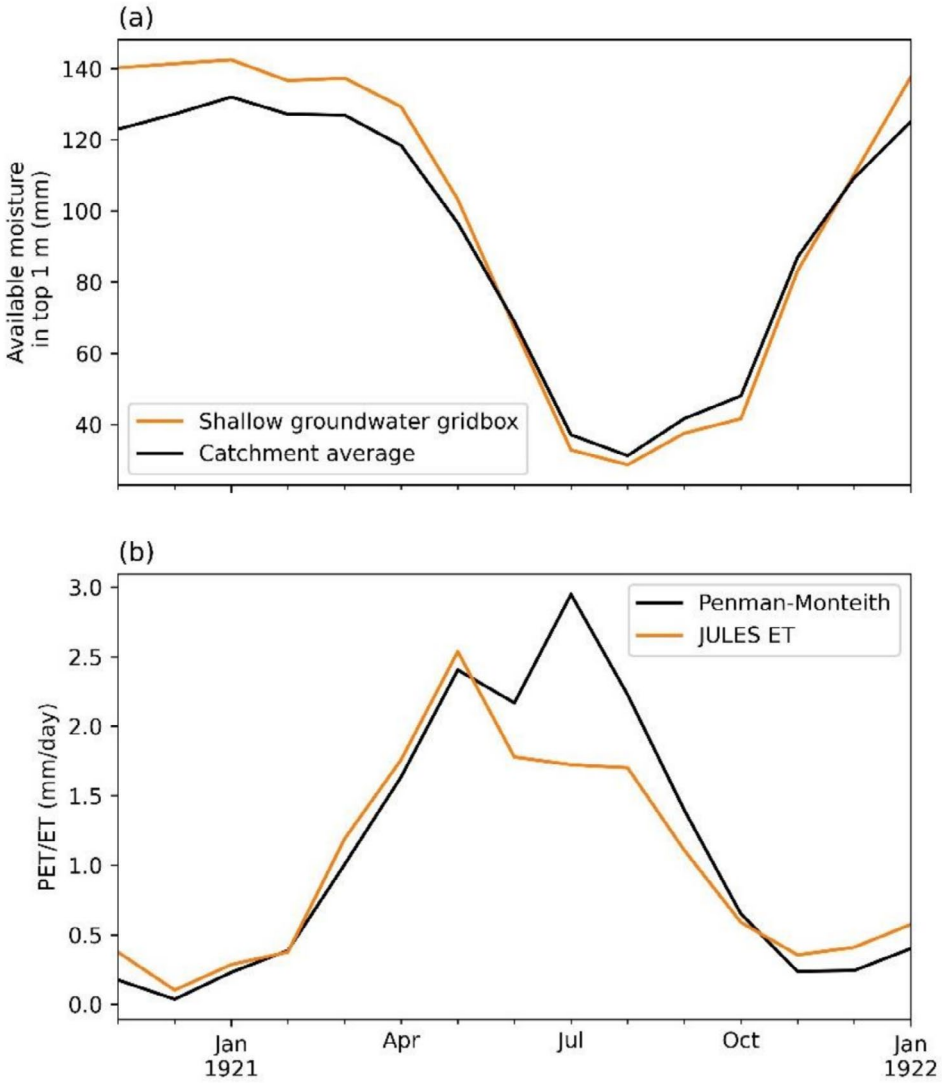

FIGURE 12 | (a) Available moisture in the uppermost 1 m of soil/chalk in a gridbox with shallow groundwater (shown in Figure 10) versus the average across the catchment. (b) Calculated FAO Penman–Monteith potential evapotranspiration (PET) versus actual evapotranspiration (ET) calculated in JULES in the same shallow groundwater gridbox. The period is the severe drought event of 1921/1922.

of the chalk matrix and fractures. The model code presented here has both benefits and limitations, depending on the application and the questions under consideration. Its limitations include the simplicity of the groundwater representation as a single-layer, albeit with exponentially decreasing hydraulic conductivity with depth, and the fact that the soil zone is always connected to the saturated zone. The computational expense of model runs does make exploring uncertainty time-consuming, although the code is planned to be parallelised. However, the model code can be used to test hypotheses that involve interactions between the saturated zone, unsaturated zone and the soil–atmosphere interaction. In the current version, river–aquifer interaction as well as abstraction can be included in any model configuration. Further, the code can be developed to include more features enabling more complex problems to be simulated.

The model code has been applied to develop a JULES configuration and after testing the model against observed river flows and groundwater levels, the model was run without abstraction for the period 1901–2015. Splitting the model into three roughly equal periods (1901–1938, 1939–1976 and 1977–2015), we found that annual ET has increased (58%, 59% and 61%) and recharge and baseflow (34%, 32% and 30%) decreased as a fraction of precipitation. The model suggests that conditions became generally drier across the 20th century with small drops in average moisture in the unsaturated zone and groundwater levels throughout all seasons. Summer ET as a fraction of rainfall was considerably higher in the third period, leading to a drier unsaturated zone in late summer/early autumn and a delay to the recharge season. The model suggests, however, there has been no increase in capillary rise from the water table to the unsaturated zone and that capillary rise is insignificant. Generally, ET is simulated as having a negative anomaly during severe droughts throughout the entire period; therefore, although the trend of drying across the 20th century may mean initial soil moisture or groundwater levels at the beginning of the drought are lower or the drought begins earlier, during the drought period any increases in PET due to climate warming are unlikely to have much impact on groundwater levels. The driver of groundwater drought in the Kennet is overwhelmingly precipitation and the influence of ET on severe drought is small.

Acknowledgements

This work was funded through the Hydro-JULES research programme of the Natural Environment Research Council (NERC) (NE/S017380/1). All the BGS authors publish with the permission of the Executive Director of the British Geological Survey (NERC). Two anonymous reviewers are thanked for improving the paper.

Funding

This work was supported by Natural Environment Research Council (NE/S017380/1).

Data Availability Statement

The standard JULES-DGW code is available at the following branch: https://code.metoffice.gov.uk/svn/jules/main/branches/dev/sarahcollins/vn5.2_dgw. The JULES-DGW code with chalk modifications can be obtained on request from the authors.

References

Alexander, L. V., and P. D. Jones. 2001. "Updated Precipitation Series for the UK and Discussion of Recent Extremes." *Atmospheric Science Letters* 1, no. 2: 142–150. https://doi.org/10.1006/asle.2001.0025.

Allen, D. J., L. J. Brewerton, L. M. Coleby, et al. 1997. *The Physical Properties of Major Aquifers in England and Wales (WD/97/034)*. British Geological Survey, 333 pp.

Bakopoulou, C. 2015. "Critical Assessment of Structure and Parameterization of JULES Land Surface Model at Different Spatial Scales in a UK Chalk Catchment." PhD thesis, Imperial College.

Barker, L. J., J. Hannaford, S. Parry, K. A. Smith, M. Tanguy, and C. Prudhomme. 2019. "Historic Hydrological Droughts 1891–2015: Systematic Characterisation for a Diverse Set of Catchments Across the UK." *Hydrology and Earth System Sciences* 23, no. 11: 4583–4602. https://doi.org/10.5194/hess-23-4583-2019.

Batelis, S. C., M. Rahman, S. Kollet, R. Woods, and R. Rosolem. 2020. "Towards the Representation of Groundwater in the Joint UK Land Environment Simulator." *Hydrological Processes* 34, no. 13: 2843–2863.

Best, M. J., M. Pryor, D. B. Clark, et al. 2011. "The Joint UK Land Environment Simulator (JULES), Model Description – Part 1: Energy and Water Fluxes." *Geoscientific Model Development* 4, no. 3: 677–699. https://doi.org/10.5194/gmd-4-677-2011.

Beven, K. J., and M. J. Kirkby. 1979. "A Physically Based, Variable Contributing Area Model of Basin Hydrology." *Hydrological Sciences Bulletin* 24, no. 1: 43–69. https://doi.org/10.1080/02626667909491834.

BGS. 2024. "Groundwater Resources in the UK." Accessed September 26, 2024. https://www.bgs.ac.uk/geology-projects/groundwater-research/groundwater-resources-in-the-uk/.

Bloomfield, J. P., B. Marchant, S. Bricker, and R. Morgan. 2015. "Regional Analysis of Groundwater Droughts Using Hydrograph Classification." *Hydrology and Earth System Sciences* 19, no. 10: 4327–4344.

Bloomfield, J. P., B. P. Marchant, and A. A. McKenzie. 2019. "Changes in Groundwater Drought Associated With Anthropogenic Warming." *Hydrology and Earth System Sciences* 23, no. 3: 1393–1408.

Bonsor, H. C., M. Shamsudduha, B. P. Marchant, A. M. MacDonald, and R. G. Taylor. 2018. "Seasonal and Decadal Groundwater Changes in African Sedimentary Aquifers Estimated Using Grace Products and LSMs." *Remote Sensing* 10, no. 6: 904. https://doi.org/10.3390/rs10060904.

Boorman, D. B., J. M. Hollis, and A. Lilly. 1995. *Hydrology of Soil Types: A Hydrologically-Based Classification of the Soils of United Kingdom*. Institute of Hydrology, IH Report no. 126, 146 pp.

Brooks, R. H., and A. T. Corey. 1964. *Hydraulic Properties of Porous Media, Hydrology Papers*. Colorado State University.

Butler, A., A. Hughes, C. Jackson, et al. 2012. "Advances in Modelling Groundwater Behaviour in Chalk Catchments." *Geological Society, London, Special Publications* 364, no. 1: 113–127.

Chan, W. C. H., T. G. Shepherd, K. Facer-Childs, G. Darch, and N. W. Arnell. 2022. "Storylines of UK Drought Based on the 2010–2012 Event." *Hydrology and Earth System Sciences* 26, no. 7: 1755–1777. https://doi.org/10.5194/hess-26-1755-2022.

Chen, Y., Y. Zhang, J. Tian, et al. 2024. "Groundwater Exhibits Spatially Opposing Trends During the Australian Millennium Drought." *Environmental Research Letters* 19, no. 7: 074016. https://doi.org/10.1088/1748-9326/ad521d.

Chu, H., D. D. Baldocchi, R. John, S. Wolf, and M. Reichstein. 2017. "Fluxes All of the Time? A Primer on the Temporal Representativeness of FLUXNET." *Journal of Geophysical Research: Biogeosciences* 122, no. 2: 289–307. https://doi.org/10.1002/2016JG003576.

Clark, D. B., and N. Gedney. 2008. "Representing the Effects of Subgrid Variability of Soil Moisture on Runoff Generation in a Land Surface Model." *Journal of Geophysical Research* 113: D10111. https://doi.org/10.1029/2007JD008940.

Clark, D. B., L. M. Mercado, S. Sitch, et al. 2011. "The Joint UK Land Environment Simulator (JULES), Model Description – Part 2: Carbon Fluxes and Vegetation Dynamics." *Geoscientific Model Development* 4, no. 3: 701–722. https://doi.org/10.5194/gmd-4-701-2011.

Collins, S. L., V. Christelis, C. R. Jackson, M. M. Mansour, D. M. Macdonald, and A. K. Barkwith. 2020. "Towards Integrated Flood Inundation Modelling in Groundwater-Dominated Catchments." *Journal of Hydrology* 591: 125755. https://doi.org/10.1016/j.jhydrol.2020.125755.

Collins, S. L., S. E. Loveless, S. Muddu, et al. 2020. "Groundwater Connectivity of a Sheared Gneiss Aquifer in the Cauvery River Basin, India." *Hydrogeology Journal* 28, no. 4: 1371–1388. https://doi.org/10.1007/s10040-020-02140-y.

Dai, A. 2011. "Characteristics and Trends in Various Forms of the Palmer Drought Severity Index During 1900–2008." *Journal of Geophysical Research: Atmospheres* 116, no. D12: D12115. https://doi.org/10.1029/2010JD015541.

Dolman, A. J., and R. A. M. de Jeu. 2010. "Evaporation in Focus." *Nature Geoscience* 3, no. 5: 296. https://doi.org/10.1038/ngeo849.

Fan, Y., G. Miguez-Macho, C. P. Weaver, R. Walko, and A. Robock. 2007. "Incorporating Water Table Dynamics in Climate Modeling: 1. Water Table Observations and Equilibrium Water Table Simulations." *Journal of Geophysical Research: Atmospheres* 112: D10125. https://doi.org/10.1029/2006JD008111.

FAO/IIASA/ISRIC/ISS-CAS/JRC. 2012. *Harmonized World Soil Database (Version 1.2)*. FAO and IIASA.

Farahmand, A., and A. AghaKouchak. 2015. "A Generalized Framework for Deriving Nonparametric Standardized Drought Indicators." *Advances in Water Resources* 76: 140–145. https://doi.org/10.1016/j.advwatres.2014.11.012.

Foster, S., J. Gathu, M. Eichholz, and R. Hirata. 2020. "Climate Change: The Utility Groundwater Role in Supply Security. The Source, April 2020, 50–54." Accessed September 27, 2024. www.thesourcemagazine.org/climate-change-the-utility-groundwater-role-in-supply-security/.

Gleeson, T., Y. Wada, M. F. P. Bierkens, and L. P. H. van Beek. 2012. "Water Balance of Global Aquifers Revealed by Groundwater Footprint." *Nature* 488, no. 7410: 197–200. https://doi.org/10.1038/nature11295.

Glendell, M., K. Blackstock, K. Adams, et al. 2024. "Future Predictions of Water Scarcity in Scotland: Impact on Distilleries and Agricultural Abstractors." CRW2023_05. Centre of Expertise for Waters (CREW). Accessed June 20, 2024. crew.ac.uk/publications.

Government Office for Science. 2024. "What Do We Know About the Future of Rainfall Capture in the UK, How It Affects General Hydrology, and the Consequences for Supply?" Accessed September 27, 2024. https://www.gov.uk/government/publications/future-of-rainfall-capture-in-the-uk/what-do-we-know-about-the-future-of-rainfall-capture-in-the-uk-how-it-affects-general-hydrology-and-the-consequences-for-supply-html#:~:text=1.1%20Rainfall%20trends%3A,in%20one%20region%20of%20UK.

Gu, L., J. Yin, L. J. Slater, et al. 2023. "Intensification of Global Hydrological Droughts Under Anthropogenic Climate Warming." *Water Resources Research* 59, no. 1: e2022WR032997. https://doi.org/10.1029/2022WR032997.

Gupta, A., A. Rico-Medina, and A. I. Caño-Delgado. 2020. "The Physiology of Plant Responses to Drought." *Science* 368, no. 6488: 266–269. https://doi.org/10.1126/science.aaz7614.

Hari, V., O. Rakovec, Y. Markonis, M. Hanel, and R. Kumar. 2020. "Increased Future Occurrences of the Exceptional 2018–2019 Central European Drought Under Global Warming." *Scientific Reports* 10, no. 1: 12207. https://doi.org/10.1038/s41598-020-68872-9.

He, Q.-L., J.-L. Xiao, and W.-Y. Shi. 2022. "Responses of Terrestrial Evapotranspiration to Extreme Drought: A Review." *Water* 14, no. 23: 3847. https://doi.org/10.3390/w14233847.

HRL. 2024. "Standardized Drought Analysis Toolbox (SDAT)." MATLAB Central File Exchange. https://www.mathworks.com/matlabcentral/fileexchange/51081-standardized-drought-analysis-toolbox-sdat.

IPCC. 2023. "Sections." In *Climate Change 2023: Synthesis Report. Contribution of Working Groups I, II and III to the Sixth Assessment Report of the Intergovernmental Panel on Climate Change*, edited by H. Lee and J. Romero, 35–115. IPCC. https://doi.org/10.59327/IPCC/AR6-9789291691647.

Ireson, A., and A. Butler. 2011. "Controls on Preferential Recharge to Chalk Aquifers." *Journal of Hydrology* 398, no. 1–2: 109–123.

Ireson, A., S. Mathias, H. Wheater, A. Butler, and J. Finch. 2009. "A Model for Flow in the Chalk Unsaturated Zone Incorporating Progressive Weathering." *Journal of Hydrology* 365, no. 3–4: 244–260.

Ireson, A., H. Wheater, A. Butler, S. Mathias, J. Finch, and J. Cooper. 2006. "Hydrological Processes in the Chalk Unsaturated Zone–Insights From an Intensive Field Monitoring Programme." *Journal of Hydrology* 330, no. 1–2: 29–43.

Jackson, C. R. 2012. "Simple Automatic Time-Stepping for Improved Simulation of Groundwater Hydrographs." *Groundwater* 50, no. 5: 736–745. https://doi.org/10.1111/j.1745-6584.2011.00898.x.

Jackson, C. R., J. P. Bloomfield, and J. D. Mackay. 2015. "Evidence for Changes in Historic and Future Groundwater Levels in the UK." *Progress in Physical Geography: Earth and Environment* 39, no. 1: 49–67. https://doi.org/10.1177/0309133314550668.

Jackson, C. R., A. G. Hughes, and M. M. Mansour. 2006a. "Conceptualisation of Groundwater Flow in the Chalk Aquifer Around Gatehampton." British Geological Survey Commissioned Report, CR/06/206C.

Jackson, C. R., A. G. Hughes, and M. M. Mansour. 2006b. "Numerical Modelling of Groundwater Flow to Thames Water Utility Ltd's Gatehampton Source." British Geological Survey Commissioned Report, CR/06/205C.

Jackson, C. R., R. Meister, and C. Prudhomme. 2011. "Modelling the Effects of Climate Change and Its Uncertainty on UK Chalk Groundwater Resources From an Ensemble of Global Climate Model Projections." *Journal of Hydrology* 399, no. 1–2: 12–28.

Jenkins, G., M. Perry, and J. Prior. 2008. *The Climate of the UK and Recent Trends*. Met Office Hadley Centre.

Jung, M., M. Reichstein, P. Ciais, et al. 2010. "Recent Decline in the Global Land Evapotranspiration Trend due to Limited Moisture Supply." *Nature* 467, no. 7318: 951–954. https://doi.org/10.1038/nature09396.

Kay, A. L., A. Griffin, A. C. Rudd, R. M. Chapman, V. A. Bell, and N. W. Arnell. 2021. "Climate Change Effects on Indicators of High and Low River Flow Across Great Britain." *Advances in Water Resources* 151: 103909. https://doi.org/10.1016/j.advwatres.2021.103909.

Keller, V. D. J., M. Tanguy, I. Prosdocimi, et al. 2015. "CEH-GEAR: 1 km Resolution Daily and Monthly Areal Rainfall Estimates for the UK for Hydrological and Other Applications." *Earth System Science Data* 7, no. 1: 143–155. https://doi.org/10.5194/essd-7-143-2015.

Kendon, M., M. McCarthy, S. Jevrejeva, et al. 2022. "State of the UK Climate 2021." *International Journal of Climatology* 42, no. S1: 1–80. https://doi.org/10.1002/joc.7787.

Lane, R. A., G. Coxon, J. E. Freer, et al. 2019. "Benchmarking the Predictive Capability of Hydrological Models for River Flow and Flood Peak Predictions Across Over 1000 Catchments in Great Britain."

Hydrology and Earth System Sciences 23, no. 10: 4011–4032. https://doi.org/10.5194/hess-23-4011-2019.

Le Vine, N., A. Butler, N. McIntyre, and C. Jackson. 2016. "Diagnosing Hydrological Limitations of a Land Surface Model: Application of JULES to a Deep-Groundwater Chalk Basin." *Hydrology and Earth System Sciences* 20, no. 1: 143–159.

Lehner, F., E. R. Wahl, A. W. Wood, D. B. Blatchford, and D. Llewellyn. 2017. "Assessing Recent Declines in Upper Rio Grande Runoff Efficiency From a Paleoclimate Perspective." *Geophysical Research Letters* 44, no. 9: 4124–4133. https://doi.org/10.1002/2017GL073253.

Liu, J., B. Wang, M. A. Cane, S. Y. Yim, and J. Y. Lee. 2013. "Divergent Global Precipitation Changes Induced by Natural Versus Anthropogenic Forcing." *Nature* 493, no. 7434: 656–659.

Liu, Y., M. Kumar, G. G. Katul, X. Feng, and A. G. Konings. 2020. "Plant Hydraulics Accentuates the Effect of Atmospheric Moisture Stress on Transpiration." *Nature Climate Change* 10, no. 7: 691–695. https://doi.org/10.1038/s41558-020-0781-5.

MacDonald, A. M., and D. J. Allen. 2001. "Aquifer Properties of the Chalk of England." *Quarterly Journal of Engineering Geology and Hydrogeology* 34: 371–384.

Marsh, T., G. Cole, and R. Wilby. 2007. "Major droughts in England and Wales, 1800–2006." *Weather* 62: 87–93. https://doi.org/10.1002/wea.67.

Martínez-de la Torre, A., E. M. Blyth, and G. P. Weedon. 2019. "Using Observed River Flow Data to Improve the Hydrological Functioning of the JULES Land Surface Model (vn4.3) Used for Regional Coupled Modelling in Great Britain (UKC2)." *Geoscientific Model Development* 12, no. 2: 765–784. https://doi.org/10.5194/gmd-12-765-2019.

Martínez-de la Torre, A., and G. Miguez-Macho. 2019. "Groundwater Influence on Soil Moisture Memory and Land–Atmosphere Fluxes in the Iberian Peninsula." *Hydrology and Earth System Sciences* 23, no. 12: 4909–4932. https://doi.org/10.5194/hess-23-4909-2019.

Mathias, S. A., A. P. Butler, N. McIntyre, and H. S. Wheater. 2005. "The Significance of Flow in the Matrix of the Chalk Unsaturated Zone." *Journal of Hydrology* 310, no. 1: 62–77. https://doi.org/10.1016/j.jhydrol.2004.12.009.

Met Office, D. Hollis, M. McCarthy, et al. 2018. *HadUK-Grid Gridded and Regional Average Climate Observations for the UK*. Centre for Environmental Data Analysis. Accessed September 27, 2024. http://catalogue.ceda.ac.uk/uuid/4dc8450d889a491ebb20e724debe2dfb.

Miguez-Macho, G., Y. Fan, C. P. Weaver, R. Walko, and A. Robock. 2007. "Incorporating Water Table Dynamics in Climate Modeling: 2. Formulation, Validation, and Soil Moisture Simulation." *Journal of Geophysical Research: Atmospheres* 112, no. D13. https://doi.org/10.1029/2006JD008112.

Milly, P. C. D., and K. A. Dunne. 2016. "Potential Evapotranspiration and Continental Drying." *Nature Climate Change* 6, no. 10: 946–949. https://doi.org/10.1038/nclimate3046.

Moore, R. J. 2007. "The PDM Rainfall-Runoff Model." *Hydrology and Earth System Sciences* 11, no. 1: 483–499. https://doi.org/10.5194/hess-11-483-2007.

Mueller, B., S. I. Seneviratne, C. Jimenez, et al. 2011. "Evaluation of Global Observations-Based Evapotranspiration Datasets and IPCC AR4 Simulations." *Geophysical Research Letters* 38, no. 6. https://doi.org/10.1029/2010GL046230.

Mukherjee, S., A. K. Mishra, M. Ashfaq, and S.-C. Kao. 2022. "Relative Effect of Anthropogenic Warming and Natural Climate Variability to Changes in Compound Drought and Heatwaves." *Journal of Hydrology* 605: 127396. https://doi.org/10.1016/j.jhydrol.2021.127396.

Niu, G. Y., Z. L. Yang, R. E. Dickinson, L. E. Gulden, and H. Su. 2007. "Development of a Simple Groundwater Model for Use in Climate Models and Evaluation With Gravity Recovery and Climate Experiment Data." *Journal of Geophysical Research* 112: D07103. https://doi.org/10.1029/2006JD007522.

Novick, K. A., D. L. Ficklin, P. C. Stoy, et al. 2016. "The Increasing Importance of Atmospheric Demand for Ecosystem Water and Carbon Fluxes." *Nature Climate Change* 6, no. 11: 1023–1027. https://doi.org/10.1038/nclimate3114.

NRW. 2024. "How We Can All Help Protect Groundwater in Wales." Accessed September 26, 2024. https://naturalresources.wales/guidance-and-advice/environmental-topics/water-management-and-quality/how-we-can-all-help-protect-groundwater-in-wales/?lang=en.

Padrón, R. S., L. Gudmundsson, B. Decharme, et al. 2020. "Observed Changes in Dry-Season Water Availability Attributed to Human-Induced Climate Change." *Nature Geoscience* 13, no. 7: 477–481. https://doi.org/10.1038/s41561-020-0594-1.

Parry, S., J. D. Mackay, T. Chitson, et al. 2024. "Divergent Future Drought Projections in UK River Flows and Groundwater Levels." *Hydrology and Earth System Sciences* 28, no. 3: 417–440. https://doi.org/10.5194/hess-28-417-2024.

Price, M., R. Downing, and W. Edmunds. 1993. "The Chalk as an Aquifer." In *The Hydrogeology of the Chalk of North-West Europe*, edited by R. A. Downing, M. Price, and G. P. Jones, 35–58. Clarendon Press.

Rahman, M., and R. Rosolem. 2017. "Towards a Simple Representation of Chalk Hydrology in Land Surface Modelling." *Hydrology and Earth System Sciences* 21, no. 1: 459–471.

Robinson, E. L., E. M. Blyth, D. B. Clark, E. Comyn-Platt, and A. C. Rudd. 2020. "Climate Hydrology and Ecology Research Support System Meteorology Dataset for Great Britain (1961–2017) [chess-met]." https://doi.org/10.5285/2ab15bf0-ad08-415c-ba64-831168be7293.

Robinson, E. L., E. M. Blyth, D. B. Clark, J. Finch, and A. C. Rudd. 2017. "Trends in Atmospheric Evaporative Demand in Great Britain Using High-Resolution Meteorological Data." *Hydrology and Earth System Sciences* 21: 1189–1224. https://doi.org/10.5194/hess-21-1189-2017.

Rowland, C. S., R. D. Morton, L. Carrasco, G. McShane, A. W. Neil, and C. M. Wood. 2017. "Land Cover Map 2015 (1 km Percentage Target Class, gb)." https://doi.org/10.5285/505d1e0c-ab60-4a60-b448-68c5bbae403e.

Rudd, A. C., V. A. Bell, and A. L. Kay. 2017. "National-Scale Analysis of Simulated Hydrological Droughts (1891–2015)." *Journal of Hydrology* 550: 368–385. https://doi.org/10.1016/j.jhydrol.2017.05.018.

Rushton, K. R., B. J. Connorton, and L. M. Tomlinson. 1989. "Estimation of the Groundwater Resources of the Berkshire Downs Supported by Mathematical Modeling." *Quarterly Journal of Engineering Geology* 22, no. 4: 329–341. https://doi.org/10.1144/GSL.QJEG.1989.022.04.06.

Rushton, K. R., and K. S. Rathod. 1981. "Aquifer Response due to Zones of Higher Permeability and Storage Coefficient." *Journal of Hydrology* 50: 299–316. https://doi.org/10.1016/0022-1694(81)90075-5.

Scanlon, B. R., S. Fakhreddine, A. Rateb, et al. 2023. "Global Water Resources and the Role of Groundwater in a Resilient Water Future." *Nature Reviews Earth & Environment* 4, no. 2: 87–101. https://doi.org/10.1038/s43017-022-00378-6.

Scanlon, B. R., A. Rateb, A. Anyamba, et al. 2022. "Linkages Between Grace Water Storage, Hydrologic Extremes, and Climate Teleconnections in Major African Aquifers." *Environmental Research Letters* 17, no. 1: 014046. https://doi.org/10.1088/1748-9326/ac3bfc.

Scheff, J., and D. M. Frierson. 2014. "Scaling Potential Evapotranspiration With Greenhouse Warming." *Journal of Climate* 27, no. 4: 1539–1558.

Seneviratne, S. I., T. Corti, E. L. Davin, et al. 2010. "Investigating Soil Moisture–Climate Interactions in a Changing Climate: A Review." *Earth-Science Reviews* 99, no. 3: 125–161. https://doi.org/10.1016/j.earscirev.2010.02.004.

Seneviratne, S. I., I. Lehner, J. Gurtz, et al. 2012. "Swiss Prealpine Rietholzbach Research Catchment and Lysimeter: 32 Year Time Series and 2003 Drought Event." *Water Resources Research* 48: W06526. https://doi.org/10.1029/2011WR011749.

Sheffield, J., E. F. Wood, and M. L. Roderick. 2012. "Little Change in Global Drought Over the Past 60 Years." *Nature* 491, no. 7424: 435–438. https://doi.org/10.1038/nature11575.

Spinoni, J., P. Barbosa, E. Bucchignani, et al. 2021. "Global Exposure of Population and Land-Use to Meteorological Droughts Under Different Warming Levels and Ssps: A Cordex-Based Study." *International Journal of Climatology* 41, no. 15: 6825–6853. https://doi.org/10.1002/joc.7302.

Taylor, R. G., B. Scanlon, P. Döll, et al. 2013. "Ground Water and Climate Change." *Nature Climate Change* 3, no. 4: 322–329. https://doi.org/10.1038/nclimate1744.

Teuling, A. J., A. F. Van Loon, S. I. Seneviratne, et al. 2013. "Evapotranspiration Amplifies European Summer Drought." *Geophysical Research Letters* 40, no. 10: 2071–2075. https://doi.org/10.1002/grl.50495.

Trenberth, K. E., A. Dai, G. van der Schrier, et al. 2014. "Global Warming and Changes in Drought." *Nature Climate Change* 4, no. 1: 17–22. https://doi.org/10.1038/nclimate2067.

UNESCO. 2015. *The United Nations World Water Development Report 2015: Water for a Sustainable World*. Vol. 1. UNESCO Publishing.

United Nations. 2022. *The United Nations World Water Development Report 2022: Groundwater: Making the Invisible Visible*. UNESCO.

Upton, K. A., C. R. Jackson, A. P. Butler, and M. A. Jones. 2020. "An Integrated Modelling Approach for Assessing the Effect of Multiscale Complexity on Groundwater Source Yields." *Journal of Hydrology* 588: 125113. https://doi.org/10.1016/j.jhydrol.2020.125113.

van Genuchten, M. T. 1980. "A Closed-Form Equation for Predicting the Hydraulic Conductivity of Unsaturated Soils." *Soil Science Society of America Journal* 44, no. 5: 892–898. https://doi.org/10.2136/sssaj1980.03615995004400050002x.

Van Loon, A. F. 2015. "Hydrological Drought Explained." *WIREs Water* 2, no. 4: 359–392. https://doi.org/10.1002/wat2.1085.

Wang, H., L. Cao, X. Li, R. Feng, and P. Zheng. 2022. "Differences in Drought Evolution as Portrayed for China Using Various Evapotranspiration Models and Drought Indices." *International Journal of Climatology* 42, no. 16: 9404–9429. https://doi.org/10.1002/joc.7829.

Weedon, G. P., S. Gomes, P. Viterbo, et al. 2011. "Creation of the Watch Forcing Data and Its Use to Assess Global and Regional Reference Crop Evaporation Over Land During the Twentieth Century." *Journal of Hydrometeorology* 12, no. 5: 823–848. https://doi.org/10.1175/2011JHM1369.1.

Wheater, H. S., D. Peach, and A. Binley. 2007. "Characterising Groundwater-Dominated Lowland Catchments: The UK Lowland Catchment Research Programme (LOCAR)." *Hydrology and Earth System Sciences* 11, no. 1: 108–124. https://doi.org/10.5194/hess-11-108-2007.

Williams, K., and D. B. Clark. 2014. *Disaggregation of Daily Data in JULES*. Met Office. 26 pp., Hadley Centre Technical Note 96.

Wösten, J. H. M., A. Lilly, A. Nemes, and C. Le Bas. 1999. "Development and Use of a Database of Hydraulic Properties of European Soils." *Geoderma* 90, no. 3: 169–185. https://doi.org/10.1016/S0016-7061(98)00132-3.

Zehe, E., T. Maurer, J. Ihringer, and E. Plate. 2001. "Modeling Water Flow and Mass Transport in a Loess Catchment." *Physics and Chemistry of the Earth, Part B: Hydrology, Oceans and Atmosphere* 26, no. 7: 487–507. https://doi.org/10.1016/S1464-1909(01)00041-7.

Zhao, C., F. Brissette, J. Chen, and J.-L. Martel. 2020. "Frequency Change of Future Extreme Summer Meteorological and Hydrological Droughts Over North America." *Journal of Hydrology* 584: 124316. https://doi.org/10.1016/j.jhydrol.2019.124316.

Zhao, M. A. G, Y. Liu, and A. G. Konings. 2022. "Evapotranspiration Frequently Increases During Droughts." *Nature Climate Change* 12, no. 11: 1024–1030. https://doi.org/10.1038/s41558-022-01505-3.

Zhao, Z., X. Hao, X. Fan, J. Zhang, S. Zhang, and X. Li. 2023. "Actual Evapotranspiration Dominates Drought in Central Asia." *Remote Sensing* 15, no. 18: 4557. https://www.mdpi.com/2072-4292/15/18/4557.